

# CUL-2LRR-1 and UBXN-3 drive replisome disassembly during DNA replication termination and mitosis

Sonnerville, Remi; Priego Moreno, Sara; Knebel, Axel; Johnson, Clare; Hastle, C. James; Gartner, Anton; Gambus, Agnieszka; Labib, Karim

DOI:

[10.1038/ncb3500](https://doi.org/10.1038/ncb3500)

License:

None: All rights reserved

Document Version

Peer reviewed version

Citation for published version (Harvard):

Sonnerville, R, Priego Moreno, S, Knebel, A, Johnson, C, Hastle, CJ, Gartner, A, Gambus, A & Labib, K 2017, 'CUL-2LRR-1 and UBXN-3 drive replisome disassembly during DNA replication termination and mitosis', *Nature Cell Biology*, vol. 19, pp. 468–479. <https://doi.org/10.1038/ncb3500>

[Link to publication on Research at Birmingham portal](#)

## Publisher Rights Statement:

Title: CUL-2LRR-1 and UBXN-3 drive replisome disassembly during DNA replication termination and mitosis, by Remi Sonnevill, Sara Priego Moreno, Axel Knebel, Clare Johnson, C. James Hastie, Anton Gartner, published in *Nature Cell Biology*, by Nature Publishing Group, first online Apr 3, 2017, doi:10.1038/ncb3500.

Copyright © 2017, Rights Managed by Nature Publishing Group

Eligibility for repository: Checked on 10/4/2017

## General rights

Unless a licence is specified above, all rights (including copyright and moral rights) in this document are retained by the authors and/or the copyright holders. The express permission of the copyright holder must be obtained for any use of this material other than for purposes permitted by law.

- Users may freely distribute the URL that is used to identify this publication.
- Users may download and/or print one copy of the publication from the University of Birmingham research portal for the purpose of private study or non-commercial research.
- User may use extracts from the document in line with the concept of 'fair dealing' under the Copyright, Designs and Patents Act 1988 (?)
- Users may not further distribute the material nor use it for the purposes of commercial gain.

Where a licence is displayed above, please note the terms and conditions of the licence govern your use of this document.

When citing, please reference the published version.

## Take down policy

While the University of Birmingham exercises care and attention in making items available there are rare occasions when an item has been uploaded in error or has been deemed to be commercially or otherwise sensitive.

If you believe that this is the case for this document, please contact [UBIRA@lists.bham.ac.uk](mailto:UBIRA@lists.bham.ac.uk) providing details and we will remove access to the work immediately and investigate.

1 **CUL-2<sup>LRR-1</sup> and UBXN-3/FAF1 drive replisome disassembly during DNA**  
2 **replication termination and mitosis**

3

4 **Remi Sonnevile<sup>1</sup>, Sara Priego Moreno<sup>2</sup>, Axel Knebel<sup>1</sup>, Clare Johnson<sup>1</sup>,**  
5 **C. James Hastie<sup>1</sup>, Anton Gartner<sup>3</sup>, Agnieszka Gambus<sup>2</sup> and Karim Labib<sup>1</sup>**

6

7 <sup>1</sup>MRC Protein Phosphorylation and Ubiquitylation Unit, School of Life  
8 Sciences, University of Dundee, Dow Street, Dundee, DD1 5EH, U.K.

9 <sup>2</sup>Institute of Cancer and Genomic Sciences, College of Medical and Dental  
10 Sciences, University of Birmingham, Edgbaston, Birmingham, B15 2TT, U.K.

11 <sup>3</sup>Centre for Gene Regulation and Expression, School of Life Sciences,  
12 University of Dundee, Dow Street, Dundee, DD1 5EH, U.K.

13

14 Correspondence should be addressed to [a.gambus@bham.ac.uk](mailto:a.gambus@bham.ac.uk) or  
15 [kpmlabib@dundee.ac.uk](mailto:kpmlabib@dundee.ac.uk).

16

## 1   **Abstract**

2           Replisome disassembly is the final step of DNA replication in  
3   eukaryotes, involving the ubiquitylation and CDC48-dependent dissolution of  
4   the CMG helicase (Cdc45-MCM-GINS). Using *Caenorhabditis elegans* early  
5   embryos and *Xenopus* egg extracts, we show that the E3 ligase CUL-2<sup>LRR-1</sup>  
6   associates with the replisome and drives ubiquitylation and disassembly of  
7   CMG, together with the CDC-48 co-factors UFD-1 and NPL-4. Removal of  
8   CMG from chromatin in frog egg extracts requires CUL2 neddylation, and our  
9   data identify chromatin recruitment of CUL2<sup>LRR1</sup> as a key regulated step during  
10   DNA replication termination. Interestingly, however, CMG persists on  
11   chromatin until prophase in worms that lack CUL-2<sup>LRR-1</sup>, but is then removed  
12   by a mitotic pathway that requires the CDC-48 co-factor UBXN-3, orthologous  
13   to the human tumour suppressor FAF1. Partial inactivation of *lrr-1* and *ubxn-3*  
14   leads to synthetic lethality, suggesting future approaches by which a deeper  
15   understanding of CMG disassembly in metazoa could be exploited  
16   therapeutically.

17

18   Keywords: DNA replication termination; replisome disassembly; CMG  
19   helicase; *Caenorhabditis elegans*; *Xenopus laevis*; Cullin; CUL-2; LRR-1;  
20   UBXN-3; FAF1; CUL2; LRR1; CDC-48, UFD-1; NPL-4; p97; VCP; ULP-4

1           Chromosome replication in eukaryotes is initiated by the assembly of  
2   the CMG helicase at origins of DNA replication<sup>1, 2</sup>. CMG then controls the  
3   progression of DNA replication forks, by unwinding the parental DNA duplex  
4   to form the single-strand substrate for DNA polymerases<sup>3, 4</sup>. The CMG  
5   helicase forms the core of the eukaryotic replisome<sup>1, 5</sup> and must remain  
6   associated with replication forks throughout elongation, since it cannot be  
7   reloaded<sup>6</sup>. The catalytic core of the helicase is formed by a hexameric ring of  
8   the MCM2-7 proteins, which is topologically trapped around the DNA template  
9   and is stabilised and activated by association with CDC45 and GINS<sup>1, 7</sup>.

10           The remarkably stable association of CMG with replication forks means  
11   that a specialized mechanism is needed to remove the helicase and trigger  
12   replisome disassembly during DNA replication termination<sup>8</sup>. In budding yeast  
13   and *Xenopus* egg extracts, the CMG helicase was found to be ubiquitylated  
14   on its Mcm7 subunit in a late step of DNA replication<sup>9-11</sup>, leading rapidly to a  
15   disassembly reaction that requires the CDC48/p97 AAA+ ATPase<sup>10, 11</sup>.

16           In *Saccharomyces cerevisiae*, the cullin 1-based E3 ligase SCF<sup>Dia2</sup>  
17   associates with the replisome and is essential for CMG ubiquitylation and  
18   disassembly<sup>10, 12, 13</sup>. Orthologues of the F-box protein Dia2 are not apparent  
19   in metazoa, but a putative role for a metazoan cullin ligase during DNA  
20   replication termination was suggested by the fact that CMG ubiquitylation and  
21   disassembly are inhibited in *Xenopus* egg extracts<sup>11</sup> by the neddylation  
22   inhibitor MLN4924<sup>14</sup>, since the major role of neddylation is to activate cullin  
23   ligases<sup>15, 16</sup>.

1           Here we describe a screen for factors controlling CMG helicase  
2   disassembly in the *C. elegans* early embryo, leading to the identification of a  
3   cullin ligase that we show is also essential for chromatin extraction of CMG  
4   during S-phase in *Xenopus* egg extracts, where we find that recruitment of the  
5   ligase to chromatin is a key regulated step during DNA replication termination.  
6   We also identify a second pathway for CMG helicase disassembly during  
7   mitosis in *C. elegans*, indicating that replisome disassembly in metazoa  
8   involves additional mechanisms not previously identified in yeast.

9

## 10   **Results**

### 11   A cytological assay for replisome dissolution in *C. elegans* early embryos

12           We established an *in vivo* assay for defects in replisome disassembly  
13   in live *C. elegans* early embryos (Figure 1), by time-lapse analysis of embryos  
14   simultaneously expressing mCherry-Histone H2B and GFP-tagged CMG  
15   components<sup>17, 18</sup>. We initially examined GFP-tagged versions of CDC-45 and  
16   the GINS component SLD-5, after depletion of CDC-48. As shown in  
17   Supplementary Figure 1a, both GFP-CDC-45 and GFP-SLD-5 were absent  
18   from chromatin during prophase in control embryos, but were chromatin-  
19   associated throughout mitosis in embryos treated with *cdc-48* RNAi. We also  
20   screened all the known or predicted adaptors of worm CDC-48<sup>19-21</sup>  
21   (Supplementary Figure 1b), and found that depletion of either subunit of the  
22   NPL-4\_UFD-1 heterodimer<sup>22, 23</sup> led to persistence of both GINS and CDC-45  
23   on condensing prophase chromatin (Figure 1b-c, Supplementary Figure 1c,  
24   Supplementary Movies 1-2). Moreover, a fraction of GFP-MCM-3 was

1 present on chromatin during early mitosis in embryos depleted for NPL-4 or  
2 CDC-48 (Figure 1d and Supplementary Figure 1d-e, *npl-4* or *cdc-48* RNAi,  
3 'early metaphase'; note that the high concentration of MCM-2-7 in the nucleus  
4 precluded the examination of prophase chromatin). Finally, we used  
5 fluorescence recovery after photobleaching (FRAP) to confirm that *npl-4* RNAi  
6 caused 'old' CMG components to persist on chromatin after S-phase, rather  
7 than driving the premature assembly of 'new' CMG complexes (Figure 1h,  
8 Supplementary Movie 3, Supplementary Figure 1g-h). These findings  
9 indicated that CDC-48 and its co-factors NPL-4 and UFD-1 are essential for  
10 the extraction of CMG components from chromatin during S-phase in the *C.*  
11 *elegans* early embryo.

12 Consistent with these data, we found that *npl-4* RNAi led to a strong  
13 accumulation of the CMG helicase with ubiquitylated MCM-7 subunit (Figure  
14 1e-g). Ubiquitylation of CMG was reduced if the completion of DNA  
15 replication was inhibited (Supplementary Figure 1f), by RNAi depletion of the  
16 ribonucleotide reductase RNR-1 as described previously<sup>18</sup>, consistent with the  
17 idea that CMG ubiquitylation in the worm embryo is linked to DNA replication  
18 termination as in budding yeast and *Xenopus laevis*<sup>10, 11</sup>.

19

20 CUL-2<sup>LRR-1</sup> is required for ubiquitylation and disassembly of the CMG helicase  
21 during S-phase in *C. elegans*

22 The *C. elegans* genome encodes CUL-1 to CUL-5 (Supplementary  
23 Figure 2a), which are orthologues of the five cullins found in diverse metazoa,  
24 plus CUL-6 that is a paralogue of CUL-1<sup>24</sup>. Using our cytological assay for

1 CMG disassembly, we found that RNAi depletion of CUL-2 was unique in  
2 causing persistence of SLD-5 and PSF-1 on prophase chromatin (Figure 2a,  
3 Supplementary Figure 2b and Supplementary Movie 4). The same defect was  
4 observed after depletion of the RING finger protein Rbx1, which links CUL-2  
5 (and CUL-1/3/4/6) to its cognate ubiquitin conjugating enzyme, or after  
6 depletion of the worm orthologues of Elongin B and Elongin C, which connect  
7 CUL-2 (and CUL-5) to its substrate adaptors (Figure 2a; see below for Elongin  
8 B). These findings indicated that a CUL-2 ligase regulates disassembly of the  
9 CMG helicase during S-phase in *C. elegans*, probably involving ubiquitin  
10 ligase activity, since not only CUL-2 but also RBX-1 is required for removing  
11 CMG from chromatin.

12 Six different substrate adaptors of CUL-2 have been characterized in  
13 *C. elegans* (Supplementary Figure 2c), five of which are conserved in  
14 humans. We depleted each of these and found that RNAi to *lrr-1* (Leu<sup>c</sup>ine-  
15 rich repeats 1) was unique in causing GINS and CDC-45 to persist on  
16 prophase chromatin (Figure 2b, Supplementary Figure 2d and Supplementary  
17 Movie 5 for GINS; see Supplementary Figure 3d below for CDC-45).  
18 Importantly, depletion of LRR-1 also dramatically reduced CMG ubiquitylation,  
19 when replisome disassembly was blocked by *npl-4* RNAi (Figure 2c-d). These  
20 data indicated that CUL-2<sup>LRR-1</sup> regulates CMG disassembly during DNA  
21 replication termination in the *C. elegans* early embryo.

22

23 A mitotic pathway for CMG chromatin extraction requires the CDC-48 co-  
24 factor UBXN-3

1           Although CMG was initially retained on prophase chromatin following  
2   RNAi depletion of CUL-2<sup>LRR-1</sup>, both GINS and CDC-45 were then released  
3   from chromatin a few minutes before nuclear envelope breakdown in late  
4   prophase (Figure 3a, Supplementary Figure 3a, b, d, and Supplementary  
5   Movies 4-5; note that MCM-2-7 could not be examined on prophase  
6   chromatin, as discussed above). Moreover, the same was true in *lrr-1Δ* / *lrr-*  
7   1Δ homozygous embryos that lack the LRR-1 protein (Figure 3c and  
8   Supplementary Figure 3c; *lrr-1* is an essential gene in *C. elegans*, but the first  
9   embryonic cell cycles in homozygous *lrr-1Δ* embryos can be examined as  
10   described in Methods). The delayed release of CMG components from  
11   chromatin in the absence of LRR-1 was not produced by a delay in the  
12   completion of S-phase, since RNAi depletion of the catalytic or primase  
13   subunits of Pol alpha greatly extended the length of S-phase, yet did not  
14   cause CMG to persist on condensing chromatin (Figure 3a-b, *div-1* and *pol*  
15   *alpha* RNAi), consistent with our previous data<sup>17</sup>. Instead, these findings  
16   indicated that the *C. elegans* early embryo has two different pathways for  
17   CMG helicase disassembly (Supplementary Figure 3e). The first pathway  
18   acts during DNA replication termination and requires CUL-2<sup>LRR-1</sup>, whereas the  
19   second provides backup and is activated during prophase. Consistent with  
20   the existence of the second pathway, we found that depletion of LRR-1 did not  
21   cause a strong accumulation of CMG in embryo extracts, compared to  
22   depletion of NPL-4 (Figure 3d, compare samples 2 and 3). However, *lrr-1*  
23   RNAi did abrogate the basal level of CMG ubiquitylation that is seen in control  
24   embryos (Figure 3d-e, longer exposures, compare samples 1 and 2).



1 Both CMG disassembly pathways require CDC-48 / UFD-1 / NPL-4,  
2 since depletion of the latter leads to persistence of CMG on chromatin  
3 throughout mitosis (Figure 1, Supplementary Figure 1). In addition to the  
4 three 'core' co-factors that form mutually exclusive complexes with CDC-48 /  
5 p97, namely UFD-1\_NPL-4, UBXN-2 / p47 and UBXN-6 / UBXD1, eukaryotic  
6 cells also contain a range of other partners of p97 / CDC-48 that recruit the  
7 segregase to specific targets or to particular sub-cellular locations<sup>25-27</sup>  
8 (Supplementary Figure 1b). To test whether one of these links CDC-48 to the  
9 mitotic CMG disassembly pathway, we combined *Irr-1* RNAi with depletion of  
10 each of the predicted CDC-48 adaptors in *C. elegans* (see Methods), and then  
11 examined the association of CMG components with mitotic chromatin.  
12 Amongst all the tested combinations, only simultaneous depletion of LRR-1  
13 and UBXN-3 led to persistence of GFP-CDC-45, GFP-PSF-1 and GFP-SLD-5  
14 on mitotic chromatin (Figure 4a, Supplementary Figure 4a-b and  
15 Supplementary Movie 6). In contrast, these CMG components were released  
16 from chromatin before prophase in embryos treated with RNAi to *ubxn-3* alone  
17 (Figure 4a, Supplementary Figure 4a-b and Supplementary Movie 7).

18 To assay directly the level of the CMG helicase in the presence or  
19 absence of UBXN-3, we isolated GFP-PSF-1 from embryo extracts as above.  
20 Simultaneous RNAi to *ubxn-3* and *Irr-1* led to a striking accumulation of CMG,  
21 equivalent to that seen with *npl-4* RNAi (Figure 4b, compare level of CDC-45  
22 and MCM-2 associated with GINS in samples 2-4), with residual ubiquitylation  
23 of CMG as seen with *npl-4 Irr-1* RNAi (compare Figure 4b samples 3-4 with  
24 Figure 3d-e samples 3-4). Together with the imaging data described above,

these findings identify UBXN-3 as a factor required for a mitotic pathway of CMG disassembly in the *C. elegans* early embryo.

#### The SUMO protease ULP-4 modulates the mitotic CMG disassembly pathway

To screen for regulators of the mitotic CMG disassembly pathway, we combined *lrr-1* RNAi with depletion of candidate proteins, including factors that regulate cell division or genome integrity (Supplementary Table 1). These included mitotic regulators such as the Aurora B and Polo kinases AIR-2 and PLK-1, candidate ubiquitin ligases such as BRC-1 (BRCA1) and SMC-5, regulators of DNA replication such as the ATL-1 checkpoint kinase, and components of the SUMO pathway. Uniquely amongst these factors, we found that co-depletion of the SUMO protease ULP-4 with LRR-1 delayed the release of CMG components from chromatin, until at or after nuclear envelope breakdown, (Figure 4c and Supplementary Figure 4c-d). ULP-4 is the major SUMO protease during mitosis in *C. elegans*, analogous to SENP6-7 in human cells, and is present on mitotic chromosomes and at the spindle midzone<sup>28</sup>. Although *ulp-4 lrr-1* RNAi produced a less severe CMG disassembly defect than co-depletion of LRR-1 and UBXN-3, these findings indicated that the UBXN-3-dependent mitotic pathway for CMG disassembly is also modulated by ULP-4.

#### Combining defects in the S-phase and mitotic CMG disassembly pathways produces synthetic lethality

1 Previous work showed that LRR-1 is essential for germ cell formation  
2 and embryonic development in *C. elegans*<sup>29, 30</sup>. In contrast, RNAi to *ubxn-3* or  
3 *ulp-4* is tolerated without causing severe embryonic lethality (see below),  
4 indicating that the mitotic CMG disassembly pathway is dispensable in worms  
5 that can disassemble CMG via the CUL-2<sup>LRR-1</sup> S-phase pathway.

6 To explore the physiological importance of the mitotic CMG  
7 disassembly pathway should CUL-2<sup>LRR-1</sup> fail to act, we fed worms on bacteria  
8 with 10% expressing *lrr-1* RNAi (Figure 4d shows that this low dose of *lrr-1*  
9 RNAi scarcely affects viability), and then gradually increased the proportion of  
10 bacteria that expressed RNAi to *ubxn-3* or *ulp-4*. Strikingly, even the lowest  
11 tested dose of *ubxn-3* RNAi produced 100% lethality in combination with 10%  
12 *lrr-1* RNAi, despite both single RNAi treatments causing almost no detectable  
13 lethality (Figure 4e). Similarly, the lowest tested dose of *ulp-4* RNAi produced  
14 90% embryonic lethality in combination with 10% *lrr-1* RNAi, even though  
15 neither individual RNAi treatment affected viability to a significant degree  
16 (Figure 4f). These findings indicate that both UBXM-3 and ULP-4 become  
17 essential when the function of CUL-2<sup>LRR-1</sup> is even partially defective,  
18 consistent with the possibility that the mitotic CMG disassembly pathway  
19 provides an essential back up for the S-phase pathway (though this remains  
20 to be demonstrated directly in future studies).

21

22 LRR-1 couples the CUL-2<sup>LRR-1</sup> ubiquitin ligase to the worm replisome

23 To test whether CUL-2<sup>LRR-1</sup> associates with the worm replisome, we  
24 treated control and *GFP-psf-1* worms with *npl-4* RNAi to block replisome

1 disassembly, and then used isolated embryos to generate extracts that were  
2 incubated with beads coupled to anti-GFP antibodies. A fraction of the  
3 resultant material was analysed by immunoblotting, to confirm the specific  
4 isolation of ubiquitylated CMG helicase from the *GFP-psf-1* embryos (Figure  
5 5a). The remainder was resolved by SDS-PAGE (Figure 5b) and analysed by  
6 mass spectrometry (Supplementary Table 2).

7         The worm CMG helicase and associated factors showed remarkable  
8 convergence with the better-characterized replisome from budding yeast  
9 (Supplementary Table 2, Figure 5c: note that our data represent the worm  
10 replisome just after termination of DNA synthesis). Notably, CUL-2<sup>LRR-1</sup> was  
11 the only cullin ligase associated with the post-termination worm replisome  
12 (Supplementary Table 2), and we subsequently found that the presence of  
13 CUL-2 in the purified material was dependent upon LRR-1 (Figure 5d,  
14 Supplementary Table 3). Therefore, LRR-1 is required for CUL-2 to associate  
15 with the replisome in *C. elegans* early embryos.

16

17 CUL2<sup>LRR1</sup> associates with the vertebrate replisome during DNA replication  
18 termination in *Xenopus* egg extracts

19         In analogous experiments, we examined whether CUL2<sup>LRR1</sup> associated  
20 with the vertebrate replisome during DNA replication termination in *Xenopus*  
21 egg extracts. Sperm nuclei were added to an extract supplemented with a  
22 dominant negative p97 mutant as well as the neddylation inhibitor MLN4924,  
23 both of which block CMG disassembly at the end of S-phase<sup>11</sup>. After bulk  
24 DNA replication had been completed (see below), the CMG helicase was

1 isolated from the chromatin fraction by DNA digestion followed by  
2 immunoprecipitation of MCM3 (Figure 6a; non-specific IgG was used as a  
3 negative control). The resultant material was then analysed by mass  
4 spectrometry and found to contain orthologues of every component of the  
5 isolated post-termination worm replisome (Supplementary Table 4).  
6 Strikingly, the post-termination vertebrate replisome was associated with a  
7 single cullin ligase, namely CUL2<sup>LRR1</sup> (Supplementary Table 4, Figure 6b).  
8 Correspondingly, immunoprecipitation of LRR1 from digested chromatin, after  
9 inhibition of replisome disassembly with a p97 inhibitor, led to co-purification  
10 not only of CUL2 and Elongin B/C, but also of the frog replisome (Figure 6c,  
11 Supplementary Table 5). Interestingly, immunoprecipitation of LRR1 from  
12 digested chromatin under such conditions led to co-depletion of CUL2  
13 (Supplementary Figure 5a, compare flowthrough for IgG and LRR1 IPs).  
14 Therefore, these data not only demonstrate that the association of CUL2<sup>LRR1</sup>  
15 with the replisome is conserved from worms to vertebrates, but also indicate  
16 that CUL2<sup>LRR1</sup> is the major CUL2 ligase on interphase chromatin.

17       The recruitment of *Xenopus* CUL2<sup>LRR1</sup> to chromatin was dependent  
18 upon replisome assembly during the initiation of chromosome replication  
19 (Figure 6d). Moreover, the association of CUL2<sup>LRR1</sup> with chromatin was  
20 greatly increased when replisome disassembly at the end of S-phase was  
21 blocked by addition of MLN4924 to the extracts (Figure 6e: Figure 6f and  
22 Supplementary Figure 5b show that replication kinetics were not affected by  
23 MLN4924, consistent with our previous findings<sup>11</sup>). These data suggested  
24 that regulated recruitment of CUL2<sup>LRR1</sup> to chromatin is an important feature of

1 the mechanism of replisome disassembly during DNA replication termination.  
2 Correspondingly, CUL2<sup>LRR1</sup> was not recruited to chromatin if DNA synthesis  
3 and subsequent termination were blocked, by addition of the DNA polymerase  
4 inhibitor aphidicolin (Figure 6g; note that caffeine had to be added to these  
5 reactions, to prevent the S-phase checkpoint pathway from limiting the  
6 accumulation of CMG on chromatin, by blocking new initiation events).

7 To test directly whether chromatin recruitment of CUL2<sup>LRR1</sup> was linked  
8 to DNA replication termination, we either inhibited replisome disassembly after  
9 termination of DNA synthesis, by inactivating CDC48 / p97 with the small  
10 molecule inhibitor NMS873<sup>31, 32</sup>, or delayed the convergence of DNA  
11 replication forks during termination, by addition of the TOPO2 inhibitor  
12 ICRF193<sup>11, 33</sup>. Neither treatment affected the kinetics of bulk DNA synthesis  
13 (Supplementary Figure 5c), consistent with previous studies<sup>9, 11</sup>. Inhibition of  
14 p97 / CDC48 with NMS873 caused a dramatic accumulation of CMG and  
15 CUL2<sup>LRR1</sup> on chromatin (Figure 6h, NMS873). However, delaying DNA  
16 replication fork convergence with ICRF193 delayed removal of CMG  
17 components from chromatin (Figure 6h, compare CDC45 and PSF2 between  
18 control and ICRF193 treatment), but this was not associated with chromatin  
19 recruitment of CUL2<sup>LRR1</sup> (Figure 6h). These findings indicate that CUL2<sup>LRR1</sup>  
20 only associates with the replisome during the termination of DNA replication.

21

22 Active CUL2<sup>LRR1</sup> is essential for extraction of the CMG helicase from  
23 chromatin at the end of chromosome replication in *Xenopus* egg extracts

1           Depletion of frog egg extracts with antibodies to CUL2-RBX1 (Figure  
2 7a) abolished detectable chromatin recruitment of CUL2<sup>LRR1</sup> during DNA  
3 replication termination (Figure 7b), even in the presence of MLN4924 that  
4 stabilises the association of the ligase with the post-termination replisome as  
5 shown above. The kinetics of bulk DNA replication in egg extracts were not  
6 affected by CUL2 depletion (Figure 7d-e), but the release of CMG  
7 components from chromatin at the end of replication was inhibited (Figure 7f).  
8 Moreover, ubiquitylation of the MCM7 subunit of CMG was both delayed and  
9 greatly reduced under such conditions (Figure 7f, MCM7).

10           To confirm that the failure of CMG chromatin extraction was indeed due  
11 to inactivation of CUL2-RBX1, we attempted to rescue the defect by addition  
12 of recombinant CUL2-RBX1, purified from insect cells. However, we noted  
13 that LRR1 was co-depleted from extracts along with CUL2 (Figure 7c), and  
14 thus we performed the rescue experiments in the presence or absence of  
15 recombinant LRR1, expressed and purified from *E. coli*. By isolating sperm  
16 chromatin from *Xenopus* egg extracts after the completion of bulk DNA  
17 replication, we confirmed that CMG components were absent from chromatin  
18 in mock-depleted extracts that were subjected to two rounds of  
19 immunoprecipitation with rabbit IgG (Figure 7g, lane 1), whereas CMG  
20 remained on chromatin following depletion of CUL2<sup>LRR1</sup> (Figure 7g, lane 2), as  
21 shown above (Figure 7f). Crucially, the defect in CMG helicase disassembly  
22 was not rescued by addition of CUL2-RBX1 complex alone (Figure 7g, lane  
23 3), but was fully complemented by the addition of CUL2-RBX1 together with  
24 recombinant LRR1 (Figure 7g, lane 5).

1           To explore whether the E3 ligase activity of CUL2<sup>LRR1</sup> was required for  
2 CMG chromatin extraction, we tested a version of CUL2-RBX1 with a mutated  
3 neddylation site and another mutation in the interaction site with the DCN1  
4 neddyase<sup>34</sup>, since neddylation promotes cullin function in vertebrates and we  
5 previously showed that the neddylation inhibitor MLN4924 blocks CMG  
6 ubiquitylation and chromatin extraction during DNA replication termination in  
7 *Xenopus* egg extracts<sup>11</sup>. Importantly, mutated CUL2-RBX1 was not able to  
8 restore CMG chromatin extraction in CUL2-depleted extracts (Figure 7g, lane  
9 4), even when added with recombinant LRR1 (Figure 7g, lane 6).

10           These findings demonstrate that CMG helicase disassembly at the end  
11 of chromosome replication in *Xenopus* egg extracts requires LRR1 and  
12 neddylation of CUL2, indicating a requirement for active CUL2<sup>LRR1</sup>. Together  
13 with past work establishing CMG helicase disassembly as the final regulated  
14 step during chromosome replication in vertebrates<sup>9</sup>, these findings establish  
15 the ubiquitin ligase CUL2<sup>LRR1</sup> as the key enzyme in this process.

16

## 17 **Discussion**

18           Previous work showed that LRR-1 is essential for germ cell formation  
19 and embryonic development in *C. elegans*<sup>29, 30</sup>. Inactivation of *lrr-1* induces  
20 DNA damage, thereby blocking germ cell proliferation and delaying mitotic  
21 entry in the early embryo<sup>29</sup>, via the ATL-1 S-phase checkpoint pathway that is  
22 equivalent to the ATR response in vertebrates. The molecular basis for DNA  
23 damage induction in the absence of LRR-1 is poorly understood, but a recent  
24 study found that low-dose RNAi to CMG components could suppress the



1 sterility phenotype of *lrr-1*Δ worms, as well as suppressing the embryonic  
2 lethality associated with a *cul-2* temperature sensitive allele under semi-  
3 restrictive conditions<sup>35</sup>. These findings suggest that the CMG helicase is a  
4 functionally important target of CUL-2<sup>LRR-1</sup> in *C. elegans*.

5       Our data indicate that CUL2<sup>LRR1</sup> activity is required to extract CMG from  
6 chromatin during DNA replication termination, both in worms and in frog egg  
7 extracts, indicating that the role of CUL2<sup>LRR1</sup> in the S-phase pathway of CMG  
8 helicase disassembly is widely conserved in metazoa. Moreover, our data  
9 identify chromatin recruitment of CUL2<sup>LRR1</sup> as a key regulated step (Figure 6).  
10 We note that a recent study of plasmid replication in *Xenopus* egg extracts  
11 has also shown that CUL2<sup>LRR1</sup> is recruited during termination and is required  
12 for replisome disassembly<sup>36</sup>, consistent with our findings.

13       Despite metazoa and yeast using different cullin ligases to trigger  
14 replisome disassembly during termination of replication, our data highlight  
15 invariant features of the disassembly mechanism in diverse eukaryotes.  
16 Firstly, the CMG helicase is ubiquitylated on its MCM7 subunit at the end of  
17 chromosome replication in budding yeast<sup>10</sup>, worm (this study) and frog<sup>9, 11</sup>,  
18 perhaps linked to a structural change in the CMG helicase that renders it  
19 accessible to the E3 ligase during DNA replication termination. Secondly, we  
20 found that UFD-1 and NPL-4 are required for CDC-48-dependent disassembly  
21 of the CMG helicase during S-phase in *C. elegans* (Figure 1 and  
22 Supplementary 1), and UFD1-NPL4 associate with the ‘post-termination’  
23 replisome in *Xenopus* (Supplementary Table 4), consistent with previous  
24 data<sup>37</sup>. These findings indicate that UFD1 and NPL4 mediate CDC48-

1 dependent replisome disassembly in metazoa, and we predict that the same  
2 is true for budding yeast.

3       Whereas budding yeast appears to have a single pathway for CMG  
4 helicase disassembly that acts during S-phase<sup>10</sup>, our *C. elegans* data indicate  
5 that metazoa have an additional CMG disassembly mechanism that operates  
6 during mitosis and requires the UBXN-3 partner of CDC-48. Interestingly, a  
7 recent study found that depletion of UBXN-3 sensitises worm embryos to DNA  
8 replication inhibitors, consistent with a role for UBXN-3 in regulation of the  
9 replisome<sup>38</sup>. It remains to be determined in future studies whether the mitotic  
10 pathway is also controlled by an E3 ubiquitin ligase, analogous to the role of  
11 CUL-2<sup>LRR-1</sup> during S-phase, but we have found that the mitotic CMG  
12 disassembly pathway is modulated by the ULP-4 SUMO protease, which is  
13 the major desumoylase on mitotic chromosomes<sup>28</sup>. It will thus be interesting  
14 to explore whether SUMO regulates CMG helicase disassembly during  
15 mitosis, perhaps inhibiting disassembly until desumoylation by ULP-4, or  
16 whether ULP-4 acts in some other way, for example by recruiting CDC-48  
17 partners like UBXN-3 to mitotic chromatin.

18       We have found that UBXN-3 and ULP-4 become essential for viability  
19 when the function of LRR-1 is even partially compromised (Figure 4),  
20 highlighting the physiological importance of UBXN-3 and ULP-4. These  
21 findings suggest that the mitotic CMG disassembly pathway provides  
22 important backup to the DNA replication termination pathway, although at  
23 present we cannot exclude that our data also reflect other roles for LRR-1,  
24 UBXN-3 and ULP-4. Interestingly, the human FAF1 protein is orthologous to

1 UBXN-3, associates with p97-UFD1-NPL4<sup>39</sup> and is deleted or depleted in  
2 many human cancers<sup>40</sup>. Moreover, depletion of FAF1 in human cells leads to  
3 defective progression and increased stalling of DNA replication forks<sup>38</sup>.  
4 Should it be possible in the future to develop small molecule inhibitors of  
5 CUL2<sup>LRR1</sup>, our data indicate that transient or partial inhibition of the CUL2<sup>LRR1</sup>  
6 E3 ligase might cause synthetic lethality in cancer cells with defective FAF1.  
7 It is thus to be hoped that a deeper understanding of the biology of replisome  
8 disassembly during DNA replication termination will have important  
9 implications for human pathology.

10

## 11 **Acknowledgements**

12 We gratefully acknowledge the support of the Medical Research  
13 Council (core grant MC\_UU\_12016/13 for KL; award MR/K007106/1 to  
14 Agnieszka Gambus) the Wellcome Trust (reference 102943/Z/13/Z for award  
15 to KL; reference 0909444/Z/09/Z for award to Anton Gartner) and the Lister  
16 Institute (award to Agnieszka Gambus) for funding our work. We thank Julian  
17 Blow for Geminin protein, MRC PPU reagents  
18 (<https://mrcppureagents.dundee.ac.uk>) for recombinant frog LRR1 and for  
19 producing antibodies, and Tom Deegan for helpful comments on the  
20 manuscript. We also thank Lionel Pintard for providing the worm line  
21 heterozygous for *Irr-1Δ*, Chris Ponting for advice regarding orthologues of the  
22 budding yeast Dia2 protein and Johannes Walter and Emily Low for  
23 discussing unpublished findings.

1

## 2 **Author Contributions**

3 RS performed the experiments in Figures 1-5 and Figures S1-S4. SPM  
4 performed the experiments in Figures 6-7 and Figures S5. KL and Agnieszka  
5 Gambus conceived the project and designed experiments in collaboration with  
6 RS and SPM. AK and CJ produced recombinant CUL2-RBX1 and JH  
7 provided recombinant LRR1. Anton Gartner provided invaluable support in  
8 the early stages of the project. KL wrote the manuscript, with contributions  
9 and critical comments from the other authors.

10

## 11 **References**

- 12 1. Gambus, A. *et al.* GINS maintains association of Cdc45 with MCM in  
13 replisome progression complexes at eukaryotic DNA replication forks.  
14 *Nat Cell Biol* **8**, 358-366 (2006).
- 15 2. Moyer, S.E., Lewis, P.W. & Botchan, M.R. Isolation of the  
16 Cdc45/Mcm2-7/GINS (CMG) complex, a candidate for the eukaryotic  
17 DNA replication fork helicase. *Proc Natl Acad Sci U S A* (2006).
- 18 3. Bell, S.P. & Labib, K. Chromosome Duplication in *Saccharomyces*  
19 *cerevisiae*. *Genetics* **203**, 1027-1067 (2016).
- 20 4. Deegan, T.D. & Diffley, J.F. MCM: one ring to rule them all. *Curr Opin*  
21 *Struct Biol* **37**, 145-151 (2016).
- 22 5. O'Donnell, M. & Li, H. The Eukaryotic Replisome Goes Under the  
23 Microscope. *Curr Biol* **26**, R247-256 (2016).

- 1 6. Labib, K., Tercero, J.A. & Diffley, J.F.X. Uninterrupted MCM2-7 function  
2 required for DNA replication fork progression. *Science* **288**, 1643-1647  
3 (2000).
- 4 7. Ilves, I., Petojevic, T., Pesavento, J.J. & Botchan, M.R. Activation of the  
5 MCM2-7 helicase by association with Cdc45 and GINS proteins.  
6 *Molecular cell* **37**, 247-258 (2010).
- 7 8. Bell, S.P. DNA Replication. Terminating the replisome. *Science* **346**,  
8 418-419 (2014).
- 9 9. Dewar, J.M., Budzowska, M. & Walter, J.C. The mechanism of DNA  
10 replication termination in vertebrates. *Nature* **525**, 345-350 (2015).
- 11 10. Maric, M., Maculins, T., De Piccoli, G. & Labib, K. Cdc48 and a  
12 ubiquitin ligase drive disassembly of the CMG helicase at the end of  
13 DNA replication. *Science* **346**, 1253596 (2014).
- 14 11. Moreno, S.P., Bailey, R., Campion, N., Herron, S. & Gambus, A.  
15 Polyubiquitylation drives replisome disassembly at the termination of  
16 DNA replication. *Science* **346**, 477-481 (2014).
- 17 12. Maculins, T., Nkosi, P.J., Nishikawa, H. & Labib, K. Tethering of  
18 SCF(Dia2) to the Replisome Promotes Efficient Ubiquitylation and  
19 Disassembly of the CMG Helicase. *Curr Biol* **25**, 2254-2259 (2015).
- 20 13. Morohashi, H., Maculins, T. & Labib, K. The amino-terminal TPR  
21 domain of Dia2 tethers SCF(Dia2) to the replisome progression  
22 complex. *Curr Biol* **19**, 1943-1949 (2009).
- 23 14. Soucy, T.A. *et al.* An inhibitor of NEDD8-activating enzyme as a new  
24 approach to treat cancer. *Nature* **458**, 732-736 (2009).

- 1 15. Duda, D.M. *et al.* Structural insights into NEDD8 activation of cullin-  
2 RING ligases: conformational control of conjugation. *Cell* **134**, 995-  
3 1006 (2008).
- 4 16. Saha, A. & Deshaies, R.J. Multimodal activation of the ubiquitin ligase  
5 SCF by Nedd8 conjugation. *Molecular cell* **32**, 21-31 (2008).
- 6 17. Sonnevile, R., Querenet, M., Craig, A., Gartner, A. & Blow, J.J. The  
7 dynamics of replication licensing in live *Caenorhabditis elegans*  
8 embryos. *J Cell Biol* **196**, 233-246 (2012).
- 9 18. Sonnevile, R., Craig, G., Labib, K., Gartner, A. & Blow, J.J. Both  
10 Chromosome Decondensation and Condensation Are Dependent on  
11 DNA Replication in *C. elegans* Embryos. *Cell Rep* **12**, 405-417 (2015).
- 12 19. Avci, D. & Lemberg, M.K. Clipping or Extracting: Two Ways to  
13 Membrane Protein Degradation. *Trends Cell Biol* **25**, 611-622 (2015).
- 14 20. Franz, A., Ackermann, L. & Hoppe, T. Ring of Change: CDC48/p97  
15 Drives Protein Dynamics at Chromatin. *Front Genet* **7**, 73 (2016).
- 16 21. Ramadan, K., Halder, S., Wiseman, K. & Vaz, B. Strategic role of the  
17 ubiquitin-dependent segregase p97 (VCP or Cdc48) in DNA replication.  
18 *Chromosoma* (2016).
- 19 22. Meyer, H.H., Shorter, J.G., Seemann, J., Pappin, D. & Warren, G. A  
20 complex of mammalian ufd1 and npl4 links the AAA-ATPase, p97, to  
21 ubiquitin and nuclear transport pathways. *The EMBO journal* **19**, 2181-  
22 2192 (2000).

- 1 23. Mouysset, J., Kahler, C. & Hoppe, T. A conserved role of  
2 Caenorhabditis elegans CDC-48 in ER-associated protein degradation.  
3 *Journal of structural biology* **156**, 41-49 (2006).
- 4 24. Sarikas, A., Hartmann, T. & Pan, Z.Q. The cullin protein family.  
5 *Genome Biol* **12**, 220 (2011).
- 6 25. Kloppsteck, P., Ewens, C.A., Forster, A., Zhang, X. & Freemont, P.S.  
7 Regulation of p97 in the ubiquitin-proteasome system by the UBX  
8 protein-family. *Biochim Biophys Acta* **1823**, 125-129 (2012).
- 9 26. Meyer, H., Bug, M. & Bremer, S. Emerging functions of the VCP/p97  
10 AAA-ATPase in the ubiquitin system. *Nat Cell Biol* **14**, 117-123 (2012).
- 11 27. Vaz, B., Halder, S. & Ramadan, K. Role of p97/VCP (Cdc48) in  
12 genome stability. *Front Genet* **4**, 60 (2013).
- 13 28. Pelisch, F. *et al.* Dynamic SUMO modification regulates mitotic  
14 chromosome assembly and cell cycle progression in Caenorhabditis  
15 elegans. *Nature communications* **5**, 5485 (2014).
- 16 29. Merlet, J. *et al.* The CRL2LRR-1 ubiquitin ligase regulates cell cycle  
17 progression during C. elegans development. *Development* **137**, 3857-  
18 3866 (2010).
- 19 30. Starostina, N.G., Simpliciano, J.M., McGuirk, M.A. & Kipreos, E.T.  
20 CRL2(LRR-1) targets a CDK inhibitor for cell cycle control in C. elegans  
21 and actin-based motility regulation in human cells. *Developmental cell*  
22 **19**, 753-764 (2010).

- 1 31. Fullbright, G., Rycenga, H.B., Gruber, J.D. & Long, D.T. p97 Promotes  
2 a Conserved Mechanism of Helicase Unloading during DNA Cross-Link  
3 Repair. *Mol Cell Biol* **36**, 2983-2994 (2016).
- 4 32. Semlow, D.R., Zhang, J., Budzowska, M., Drohat, A.C. & Walter, J.C.  
5 Replication-Dependent Unhooking of DNA Interstrand Cross-Links by  
6 the NEIL3 Glycosylase. *Cell* **167**, 498-511 e414 (2016).
- 7 33. Cuvier, O., Stanojcic, S., Lemaitre, J.M. & Mechali, M. A topoisomerase  
8 II-dependent mechanism for resetting replicons at the S-M-phase  
9 transition. *Genes & development* **22**, 860-865 (2008).
- 10 34. Bandau, S., Knebel, A., Gage, Z.O., Wood, N.T. & Alexandru, G.  
11 UBXN7 docks on neddylated cullin complexes using its UIM motif and  
12 causes HIF1alpha accumulation. *BMC Biol* **10**, 36 (2012).
- 13 35. Ossareh-Nazari, B., Katsiarimpa, A., Merlet, J. & Pintard, L. RNAi-  
14 Based Suppressor Screens Reveal Genetic Interactions Between the  
15 CRL2LRR-1 E3-Ligase and the DNA Replication Machinery in  
16 *Caenorhabditis elegans*. *G3 (Bethesda)* (2016).
- 17 36. Dewar, J.M., Low, E., Mann, M., Raschle, M. & Walter, J.C. CRL2Lrr1  
18 promotes unloading of the vertebrate replisome from chromatin during  
19 replication termination. *Genes Dev.* **doi:10.1101/gad.291799.116**  
20 (2017).
- 21 37. Franz, A. *et al.* CDC-48/p97 coordinates CDT-1 degradation with GINS  
22 chromatin dissociation to ensure faithful DNA replication. *Mol Cell* **44**,  
23 85-96 (2011).



- 1 38. Franz, A. *et al.* Chromatin-associated degradation is defined by UBXN-  
2 3/FAF1 to safeguard DNA replication fork progression. *Nature*  
3 *communications* **7**, 10612 (2016).
- 4 39. Lee, J.J. *et al.* Complex of Fas-associated factor 1 (FAF1) with valosin-  
5 containing protein (VCP)-Npl4-Ufd1 and polyubiquitinated proteins  
6 promotes endoplasmic reticulum-associated degradation (ERAD). *J*  
7 *Biol Chem* **288**, 6998-7011 (2013).
- 8 40. Menges, C.W., Altomare, D.A. & Testa, J.R. FAS-associated factor 1  
9 (FAF1): diverse functions and implications for oncogenesis. *Cell Cycle*  
10 **8**, 2528-2534 (2009).
- 11 41. Sharrock, W.J., Sutherlin, M.E., Leske, K., Cheng, T.K. & Kim, T.Y.  
12 Two distinct yolk lipoprotein complexes from *Caenorhabditis elegans*. *J*  
13 *Biol Chem* **265**, 14422-14431 (1990).
- 14 42. Gambus, A. *et al.* A key role for Ctf4 in coupling the MCM2-7 helicase  
15 to DNA polymerase alpha within the eukaryotic replisome. *EMBO J* **28**,  
16 2992-3004 (2009).
- 17 43. Sengupta, S., van Deursen, F., de Piccoli, G. & Labib, K. Dpb2  
18 integrates the leading-strand DNA polymerase into the eukaryotic  
19 replisome. *Current biology : CB* **23**, 543-552 (2013).

20

## 1 **Figure legends**

### 2 **Figure 1**

3 The CDC-48 co-factor NPL-4 is required for CMG helicase disassembly during  
4 S-phase in the *C. elegans* early embryo. **(a)** Illustration of a live-embryo  
5 assay for CMG helicase disassembly, comparing control embryos ('normal  
6 CMG disassembly') with mutant embryos ('defective CMG disassembly').  
7 Note that the two nuclei derived from oogenesis and spermatogenesis –  
8 referred to in this manuscript as the female and male pronuclei - move  
9 together during prophase of the first cell cycle. Following nuclear envelope  
10 breakdown, the 'male' and 'female' sets of chromosomes then intermingle  
11 during metaphase. **(b)** Timelapse video microscopy of the first cell cycle in  
12 embryos expressing GFP-SLD-5 and mCherry-HistoneH2B, either untreated  
13 or exposed to *npl-4* RNAi. The female pronucleus is shown during S-phase,  
14 before convergence with the male pronucleus. Prophase begins during  
15 migration of the pronuclei. The arrows indicate examples of persistence of  
16 GFP-SLD-5 on chromatin during prophase after depletion of NPL-4. **(c)**  
17 Equivalent analysis for embryos expressing GFP-CDC-45. **(d)** Equivalent  
18 data for embryos expressing GFP-MCM-3. The arrow indicates the small pool  
19 of GFP-MCM-3 that remains on chromatin during early metaphase after  
20 depletion of NPL-4. **(e)** Homozygous *GFP-psf-1 / GFP-psf-1* worms were  
21 exposed to *npl-4* RNAi or left untreated. Embryos were then isolated and  
22 used to generate whole-embryo extracts, before immunoprecipitation of GFP-  
23 PSF-1. The indicated proteins were monitored by immunoblotting. **(f)** The  
24 same samples were separated in a 4-12% gradient gel, before immunoblotting

1 with an antibody to poly-ubiquitin chains. (g) Equivalent *npl-4* RNAi  
2 experiment comparing control worms with homozygous *mcm7-5FLAG-9His*  
3 embryos generated by CRISPR-Cas9. The samples were separated in a 3-  
4 8% gradient gel, before immunoblotting with antibody to poly-ubiquitin chains.  
5 (h) Timelapse video microscopy of an *npl-4* RNAi embryo expressing GFP-  
6 CDC-45 and mCherry-HistoneH2B. The GFP signal in the female pronucleus  
7 was photo-bleached during early S-phase and then monitored in the  
8 subsequent mitosis. Lack of recovery of the GFP signal on 'female'  
9 chromosomes, compared to the unbleached control male pronucleus,  
10 indicated that GFP-CDC45 persists on chromatin after S-phase rather than  
11 being reloaded, in embryos lacking NPL-4. The scale bars correspond to  
12 5µm. Unprocessed scans of key immunoblots are shown in Supplementary  
13 Figure 8.

14

## 15 **Figure 2**

16 CUL-2<sup>LRR-1</sup> is required for CMG helicase disassembly during S-phase in *C.*  
17 *elegans*. (a-b) Embryos from *GFP-sld-5 mCherry-H2B* worms were exposed  
18 to the indicated RNAi and processed as in Figure 1b. Timelapse images are  
19 shown from S-phase to mid-prophase. Five embryos were examined for each  
20 treatment and all behaved equivalently. Arrows denote examples of  
21 persistence of GFP-SLD-5 on prophase chromatin and scale bars correspond  
22 to 5µm. (c-d) Embryos from homozygous *GFP-psf-1 / GFP-psf-1* worms were  
23 exposed to the indicated RNAi and processed as in Figure 1e-f. Unprocessed  
24 scans of key immunoblots are shown in Supplementary Figure 8.

1

2 **Figure 3**

3 A mitotic pathway for CMG helicase disassembly is revealed in the absence of  
4 CUL-2<sup>LRR-1</sup>. (a) Embryos from *GFP-psf-1 mCherry-H2B* worms were exposed  
5 to the indicated RNAi treatments, or empty vector in the control, and then  
6 processed as in Figure 1b, except that the figure depicts data from the second  
7 embryonic cell cycle (P1 cell). Timelapse images are shown from S-phase to  
8 metaphase. GFP-PSF1 initially persists on prophase chromatin following  
9 depletion of LRR-1 (the arrows denote examples), before being released in  
10 late prophase (indicated by asterisk). Scale bars correspond to 5μm. (b) The  
11 duration of the indicated cell cycle phases for the experiment in (a) were  
12 measured as described in Methods. The data are expressed relative to the  
13 length of the corresponding period in control embryos, and represent the  
14 mean values (n = 5 embryos; the lines on the boundary of each cell cycle  
15 phase indicate standard deviations from the mean). (c) Worms homozygous  
16 for *GFP-psf-1* and *lrr-1Δ* were grown in parallel to the equivalent heterozygote  
17 (control), as described in Methods. After exposure to *atl-1* RNAi (this allows  
18 homozygous *lrr-1Δ* germ cells to proceed with meiosis), the resultant embryos  
19 were processed as above. The images depict the second embryonic cell  
20 cycle (P1 cell), showing persistent association of GFP-PSF-1 with chromatin  
21 during prophase (arrows), before release in late prophase (asterisk). (d-e)  
22 Homozygous *GFP-psf-1* worms were exposed to the indicated RNAi.  
23 Embryos were then isolated and processed as in Figure 1e-f. Unprocessed  
24 scans of key immunoblots are shown in Supplementary Figure 8.

1

2 **Figure 4**

3 The mitotic CMG helicase disassembly pathway requires UBXN-3 and is  
4 modulated by the SUMO protease ULP-4, both of which become essential  
5 when LRR-1 is depleted. (a) Embryos from *GFP-psf-1 mCherry-H2B* worms  
6 were exposed to the indicated RNAi and processed as in Figure 3a. The  
7 arrows indicate persistent association of GFP-PSF1 with mitotic chromatin  
8 (throughout mitosis in the case of RNAi to *npl-4*, or after simultaneous RNAi to  
9 *lrr-1 + ubxn-3*), whereas the asterisk denotes release of GFP-PSF-1 from  
10 chromatin in late prophase in embryos treated only with *lrr-1* RNAi. The scale  
11 bars correspond to 5 $\mu$ m. (b) Homozygous *GFP-psf-1* worms were exposed to  
12 the indicated RNAi and isolated embryos were then processed as in Figure  
13 1e. (c) Embryos from *GFP-cdc-45 mCherry-H2B* worms were exposed to the  
14 indicated RNAi and processed as above. The data correspond to the AB cell  
15 in the second cell cycle, in which *lrr-1 ulp-4* double RNAi leads to persistence  
16 of GFP-CDC-45 until at or after nuclear envelope breakdown (8 of 9 embryos  
17 tested). (d) Worms were fed on plates where the indicated proportion of  
18 bacteria expressed *lrr-1* double-stranded RNAi, and embryonic viability was  
19 measured as described in Methods (for each timepoint, 69-94 embryos were  
20 examined from five adult worms). (e) Worms were fed on the indicated  
21 proportion of bacteria expressing *ubxn-3* RNAi, either alone or in combination  
22 with 10% bacteria expressing *lrr-1* RNAi. The data represent the mean values  
23 (n = 3 independent experiments; for each timepoint, 70-100 embryos were  
24 examined from five adult worms), with the indicated standard deviations from

1 the mean value. (f) Similar experiment involving increasing doses of *ulp-4*  
2 RNAi, with or without 10% *lrr-1* RNAi (n = 3 independent experiments; for  
3 each timepoint, 70-100 embryos were examined from five adult worms).  
4 Unprocessed scans of key immunoblots are shown in Supplementary Figure  
5 8.

6

## 7 **Figure 5**

8 Isolation of the post-termination worm replisome. (a) Control or homozygous  
9 *GFP-psf-1* worms were exposed to *npl-4* RNAi before being processed as  
10 described above for Figure 4. The purified samples were monitored by SDS-  
11 PAGE and immunoblotting of the indicated components of the CMG helicase.  
12 (b) The remainder of the samples were then resolved in a 4-12% gradient gel,  
13 which was stained with colloidal coomassie. The major contaminants in both  
14 samples (marked with asterisks) represent the four major yolk proteins of the  
15 worm early embryo<sup>41</sup>. Each lane was cut into 40 bands as indicated, before  
16 analysis of protein content by mass spectrometry (see Supplementary Table  
17 2). (c) Comparison of the replisome isolated from active replication forks in  
18 budding yeast <sup>1, 42, 43</sup>, with the isolated post-termination replisome from worm  
19 and frog (this study). For simplicity, some of the proteins that act at forks, but  
20 that are not present in the isolated replisome, have been omitted. In addition,  
21 Mcm10 has been excluded, since its status at forks and its association with  
22 the isolated replisome remain unclear (absent from isolated yeast and worm  
23 replisomes under physiological conditions, but co-purifying with frog MCM-3  
24 from digested chromatin post-termination). (d) Comparison of isolated

1 replisome material for the experiment in Supplementary Table 3 (worms  
2 treated with *npl-4* RNAi or *npl-4 lrr-1* double RNAi). Unprocessed scans of  
3 key immunoblots are shown in Supplementary Figure 8.

4

## 5 **Figure 6**

6 CUL2<sup>LRR1</sup> associates with the post-termination vertebrate replisome and is  
7 recruited to chromatin during DNA replication termination in *Xenopus* egg  
8 extracts. (a) Experimental scheme for isolation of proteins associated with the  
9 CMG helicase after termination in the absence of replisome disassembly, in  
10 extracts of *Xenopus laevis* eggs. (b) Immunoblots of input and the indicated  
11 IP samples for the experiment in (a). (c) Replisome disassembly was  
12 inhibited with the p97 inhibitor NMS873, and LRR1 was then isolated from  
13 digested chromatin at the 70' timepoint, in parallel with a control IP with IgG,  
14 before detection of the indicated proteins by immunoblotting. (d) Chromatin  
15 association of the indicated factors was monitored by immunoblotting, at the  
16 indicated timepoints after addition of sperm chromatin to egg extracts (except  
17 for the -DNA sample that lacked chromatin). Where indicated, replication  
18 initiation was blocked by addition of p27(KIP1) or Geminin. The neddyase  
19 inhibitor MLN4924 was added to all samples to block replisome disassembly.  
20 (e) Timecourse experiment comparing chromatin-bound factors in the  
21 absence or presence of the neddylation inhibitor MLN4924. (f) Replication  
22 kinetics were monitored for the experiment in (e), by incorporation of  
23 radiolabelled  $\alpha$ -dATP into newly synthesised DNA (see also Supplementary  
24 Figure 5b; source data for repeats of this experiment are included in

Supplementary Table 6). **(g)** Inhibition of DNA synthesis blocks association of CUL2<sup>LRR1</sup> with chromatin. DNA synthesis was inhibited with the DNA polymerase inhibitor aphidicolin. Caffeine was added to inactivate the S-phase checkpoint, which otherwise would have reduced the level of CMG on chromatin +Aphidicolin. **(h)** Analogous experiment to that in (e), showing that CUL2-LRR1 accumulated on chromatin with CMG when replisome disassembly was blocked by the p97 inhibitor NMS873, but chromatin recruitment of CUL2-LRR1 was inhibited if DNA replication termination was delayed by addition of the TOPO2 inhibitor ICRF193. Unprocessed scans of key immunoblots are shown in Supplementary Figure 8.

11

## 12 **Figure 7**

Active CUL2<sup>LRR1</sup> is required for extraction of CMG components from chromatin during DNA replication termination in *Xenopus* egg extracts. **(a)** Experimental scheme. **(b)** Replication reactions were performed in the presence of MLN4924 to stabilise CUL2<sup>LRR1</sup> on chromatin during DNA replication termination in mock-depleted extracts (treated with two rounds of IgG-beads). In contrast, neither CUL2 nor LRR1 were detected on chromatin in CUL2-depleted extracts, confirming the efficiency of the depletion. **(c)** Depletion of CUL2 also removes LRR1 from the extract (the panel shows immunoblots of the antibody-coupled beads after each of the two rounds of depletion). **(d)** Kinetics of DNA synthesis in extracts subjected to two rounds of immunoprecipitation with control IgG ('mock depletion') or with antibodies to Hs\_CUL2-RBX1 ('CUL2 depletion', see Methods). Source data for repeats of



1 this experiment are included in Supplementary Table 6. (e) In an analogous  
2 experiment, replication reactions were performed in 'mock-depleted' and CUL-  
3 depleted extracts. A pulse of  $\alpha$ -dATP was added for 3' at either the 60' or  
4 120' timepoints, and the incorporation of radiolabel into nascent DNA was  
5 monitored after isolation of total DNA, indicating that replication proceeded  
6 and completed with similar kinetics in both extracts, consistent with the data in  
7 (d). (f) Kinetics of chromatin association of the indicated factors for the same  
8 experiment shown in (a-b). Note that the MCM7 immunoblot is over-exposed  
9 in order to reveal the ubiquitylated forms of the protein. (g) Mock-depleted or  
10 CUL2-depleted extracts were supplemented with the indicated recombinant  
11 proteins (X.l. LRR1, wt/mutant Hs\_CUL2-RBX1 – see Methods), and  
12 chromatin was isolated from the 120' timepoint in a similar experiment to that  
13 described above. Unprocessed scans of key immunoblots are shown in  
14 Supplementary Figure 8.

## 16 **Competing Financial Interests**

17 The authors confirm that they have no competing financial interests.

## Legends to Supplementary Information

### Supplementary Figure 1

The CDC-48\_UFD-1\_NPL-4 complex is required for CMG helicase disassembly in *C. elegans*. **(a)** *cdc-48* RNAi leads to persistence of GINS and CDC-45 on chromatin during prophase and throughout mitosis (examples indicated by arrows). **(b)** Adaptors of CDC-48 in *C. elegans*. **(c)** *ufd-1* RNAi leads to persistence of GINS and CDC-45 on chromatin during prophase and throughout mitosis (examples indicated by arrows). **(d)** Equivalent experiment to that in Figure 1d, illustrating the effect of *npl-4* RNAi on embryos expressing GFP-MCM-3. To help visualise the small proportion of GFP-MCM-3 on chromatin in early metaphase (marked by an arrow), the experiment also included RNAi to the 3'UTR of endogenous MCM3 (this 3' UTR is not present in the GFP-MCM-3 transgene), to increase the incorporation of GFP-MCM3 into replication complexes. **(e)** *cdc-48* RNAi experiment, analogous to that in Figure 1d. **(f)** Homozygous *GFP-psf-1* worms were exposed to the indicated RNAi. Embryos were then isolated and processed as in Figure 1e-f. The middle panels show that the amount of CMG isolated from RNR-1 depleted extract was reduced compared to control (compare levels of MCM-7, MCM-2 and CDC-45), due to the inhibition of DNA replication in each embryonic cell cycle. In the right panels, loading of the GFP-PSF-1 IP samples was adjusted to obtain a similar level of CMG (compare MCM-2 and CDC-45). **(g-h)** Photobleaching experiments for GFP-SLD5 and GFP-MCM3, equivalent to the experiment in Figure 1h. The scale bars correspond to 5 $\mu$ m. Unprocessed scans of key immunoblots are shown in Supplementary Figure 8.

## Supplementary Figure 2

CUL-2<sup>LRR-1</sup> is required for removal of GINS from chromatin during S-phase in *C. elegans*. (a) *C. elegans* contain six families of cullin complexes, each with a specific cullin and a unique set of substrate adaptors. (b) Embryos from *GFP-sld-5 mCherry-H2B* worms were exposed to RNAi against the indicated cullins and processed as in Figure 2. Timelapse images are shown from S-phase to mid-prophase. (c) Six forms of the CUL-2 ligase in *C. elegans*, each with a unique substrate adaptor. (d) Embryos from *GFP-sld-5 mCherry-H2B* worms were exposed to RNAi against the indicated substrate adaptors of CUL-2 and processed as in Figure 2. Timelapse images are shown from S-phase to mid-prophase. RNAi for *zyg-11* produces meiotic defects and leads to abnormal nuclear morphology in the first embryonic cell cycle. Arrows in this figure indicate the persistent association of GFP-SLD-5 with mitotic chromatin in embryos treated with *npl-4* RNAi. Scale bars correspond to 5 $\mu$ m.

## Supplementary Figure 3

A new pathway for CMG helicase disassembly acts during mitosis. (a) Embryos from *GFP-psf-1 mCherry-H2B* worms were exposed to the indicated RNAi and processed as in Figure 3. Timelapse images of the first embryonic cell cycle are shown from S-phase to metaphase. GFP-PSF1 initially persists on prophase chromatin following RNAi to components of CUL-2<sup>LRR-1</sup> (the arrows denote examples), before being released in late prophase (indicated by asterisks). (b) Extended timecourses for the GFP-SLD-5 data presented in

Figure 2a-b. (c) Data from the first cell cycle, for the experiment in Figure 3b. (d) Embryos from *GFP-cdc-45 mCherry-H2B* worms were exposed to the indicated RNAi and processed as above. (e) Illustration of CMG disassembly defects produced either by depletion of CDC-48 / UFD-1 / NPL-4, or by depletion of components of CUL-2<sup>LRR-1</sup>. Scale bars correspond to 5 $\mu$ m.

#### Supplementary Figure 4

The mitotic disassembly pathway for the CMG helicase requires UBXXN-3 and is modulated by ULP-4. (a) Embryos from *GFP-sld-5 mCherry-H2B* worms were exposed to the indicated RNAi and processed as in Figure 4a. The arrows indicate persistent association of GFP-PSF1 with mitotic chromatin (throughout mitosis in the case of RNAi to *npl-4*, or after simultaneous RNAi to *lrr-1 + ubxn-3*), whereas the asterisk denotes release of GFP-PSF-1 from chromatin in late prophase in embryos treated only with *lrr-1* RNAi. Scale bars correspond to 5 $\mu$ m. (b) Embryos from *GFP-cdc-45 mCherry-H2B* worms were processed as for Figure 4b. (c) Embryos from *GFP-psf-1 mCherry-H2B* worms were exposed to the indicated RNAi and processed as above. The data correspond to the AB cell in the second cell cycle and CMG components remained on chromatin until at or after nuclear envelope breakdown in 3/5 embryos treated with *lrr-1 ulp-4* double RNAi. The panel shows an example of an embryo where CMG persists on chromatin until nuclear envelope breakdown upon co-depletion of LRR-1 and ULP-4. (d) Data from a similar experiment, corresponding to the EMS cell in the third cell cycle. Note that in this case we also depleted the ATL-1 checkpoint kinase, to shorten the

otherwise long cell cycle delay that is induced by the combination of *ulp-4 lrr-1* double RNAi. CMG components remained on chromatin until late metaphase in 5/5 embryos treated with *lrr-1 ulp-4 atl-1* triple RNAi. CMG was extracted normally from chromatin during S-phase in embryos subjected to *ulp-4 atl-1* double RNAi (5/5 embryos tested), whereas *lrr-1 atl-1* double RNAi resembled *lrr-1* single RNAi treatment (CMG extracted before the end of prophase in 5/5 embryos).

### **Supplementary Figure 5**

Additional supplementary material for experiments with *Xenopus* egg extracts.

(a) In a similar experiment to that in Figure 6c, replisome disassembly was blocked during chromosome replication by addition of MLN4924 to *Xenopus* egg extracts. After isolation of chromatin and digestion of DNA, immunoprecipitation of LRR1 led to co-depletion of CUL2. (b) Analysis of ongoing DNA synthesis at the indicated timepoints for the experiment in Figure 6e-f, by addition of short pulses of  $\alpha$ -dATP (see Methods). Data for repeats of this experiment are included in Supplementary Table 6. (c) Replication kinetics for the experiment in Figure 6h, measured by monitoring total incorporation of  $\alpha$ -dATP into nascent DNA by the indicated timepoints (see Methods). Data for repeats of this experiment are included in Supplementary Table 6. Unprocessed scans of key immunoblots from this Figure are shown in Supplementary Figure 8.

### **Supplementary Figure 6**

CUL2 is very highly conserved in vertebrates. Alignment of *Xenopus* CUL2 with the human and mouse orthologues, showing that the mammalian and frog proteins are almost identical. Moreover, previous work indicated that all key residues in CUL2 that contact EloB-C and substrate adaptors are 100% conserved between the human and frog orthologues<sup>1</sup>.

### **Supplementary Figure 7**

Validation of new antibodies generated in this study for *C. elegans* proteins.

**(a-d)** In each case, RNAi was used to deplete the corresponding protein, before immunoblotting of embryonic extracts (upper panels). Ponceau S staining of the nitrocellulose membrane (lower panels) provides a loading control in each case.

### **Supplementary Figure 8**

Unprocessed scans of key immunoblots. **(a)** Raw immunoblot data for Figure 1e, with red boxes indicating the crops used to construct Figure 1e. **(b)** Equivalent data for Figure 1f. **(c)** Equivalent data for Figure 1g. **(d)** Equivalent data for Figure 6d. **(e)** Equivalent data for Figure 6h.

### **Supplementary Table 1**

Factors targeted by RNAi in screen for components of the mitotic CMG disassembly pathway.

### **Supplementary Table 2**

CUL-2<sup>LRR-1</sup> associates with the isolated 'post-termination' replisome from *C. elegans*. Summary of mass spectrometry data for experiment shown in Figure 5b.

### **Supplementary Table 3**

LRR-1 is required for CUL-2 to associate with the 'post-termination' worm replisome. Summary of mass spectrometry data for experiment shown in Supplementary Figure 5d.

### **Supplementary Table 4**

CUL2<sup>LRR1</sup> associates with the 'post-termination' frog replisome. Summary of mass spectrometry data for experiment summarised in Figure 6a.

### **Supplementary Table 5**

The 'post-termination' replisome associates with purified frog CUL2<sup>LRR1</sup>. Summary of mass spectrometry data for an equivalent experiment to that shown in Figure 6c.

### **Supplementary Table 6**

Statistics Source Data. Source data of all repeats of the experiments in Figure 6f, Figure 7d, Supplementary Figure 5b and Supplementary Figure 6g.

### **Supplementary Table 7**

Antibody dilutions for immunoblots.

### **Supplementary Table 8**

Sequence of oligonucleotide primers used to generate RNAi vectors for depletion of *C. elegans* proteins.

### **Supplementary Movie 1**

The CMG helicase component PSF-1 does not associate with condensing chromatin during mitotic prophase or throughout mitosis. Video of a single optical section through an embryo expressing GFP-PSF-1 (left panel) and mCherry-Histone H2B (right panel) progressing throughout the first and second embryonic cell cycles. Images were acquired every 10 sec with a spinning disk confocal microscope and processed with ImageJ software. The female and male pronuclei are orientated respectively towards the left and right of the video.

### **Supplementary Movie 2**

GFP-PSF-1 associates with condensing chromatin during prophase in embryos depleted for NPL-4 and remains on chromatin throughout mitosis. Images were acquired and analysed as for Supplementary Movie 1.

### **Supplementary Movie 3**

FRAP analysis of GFP-CDC-45 after depletion of NPL-4. The movie was generated as above and shows an embryo expressing GFP-CDC-45 (left panel) and mCherry-Histone H2B (right panel). The female pronucleus (left



side of the embryo) was photobleached during early S-phase (shown as a white disk in the video at 1'50") and the chromosomes from the female and male pronuclei were then analysed during the following mitosis (see 19'30" to 24'50"). No recovery of the GFP-CDC-45 signal was observed on the female chromatin, indicating that depletion of NPL-4 causes CDC-45 to persist on chromatin from S-phase until the end of mitosis.

#### **Supplementary Movie 4**

GFP-PSF-1 associates with condensing chromatin during prophase in embryos depleted for CUL-2, but is then released from chromatin during late prophase. Images were acquired and analysed as for Supplementary Movie 1. Note that depletion of CUL-2 leads to meiotic defects in the embryo and thus to abnormal nuclear morphology, reflecting the important role of CUL-2<sup>ZYG-11</sup> during the second meiotic cell division <sup>2,3</sup>. In addition, mitotic entry is delayed in the first embryonic cell cycle after depletion of CUL-2.

#### **Supplementary Movie 5**

GFP-PSF-1 associates with condensing chromatin during prophase in embryos depleted for LRR-1, but is then released from chromatin during late prophase. Images were acquired and analysed as for Supplementary Movie 1. The association of GFP-PSF-1 with prophase chromatin can be seen in the first embryonic cell cycle (P0 cell) from 3'20" to 5'50" and during the second cell cycle from 24'30" to 26'10" for the AB cell (left side of embryo) or from 27'30" to 29'10" for the P1 cell (right side).

### **Supplementary Movie 6**

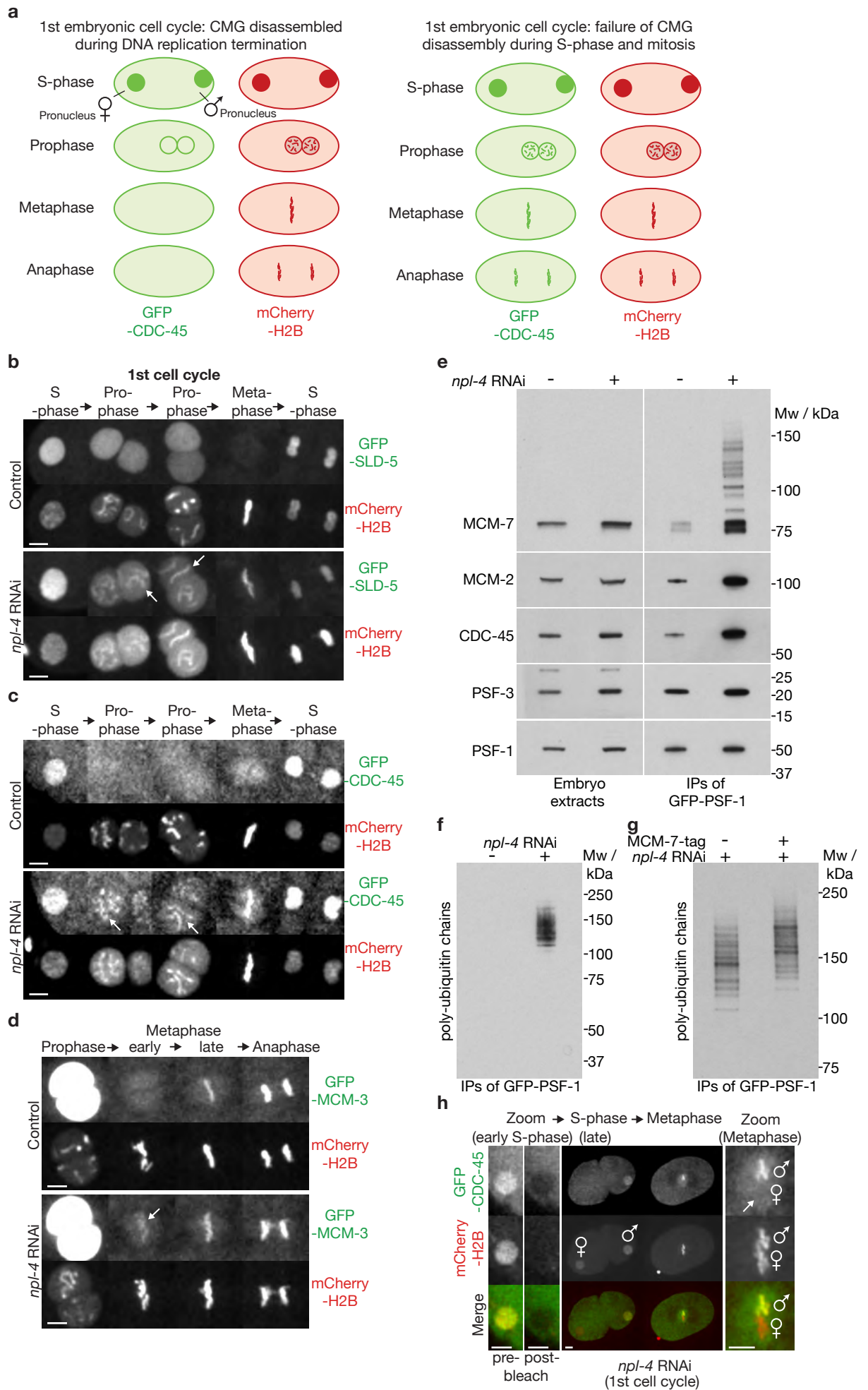
GFP-PSF-1 remains on chromatin throughout mitosis in embryos depleted for both UBXN-3 and LRR-1. Images were acquired and analysed as for Supplementary Movie 1.

### **Supplementary Movie 7**

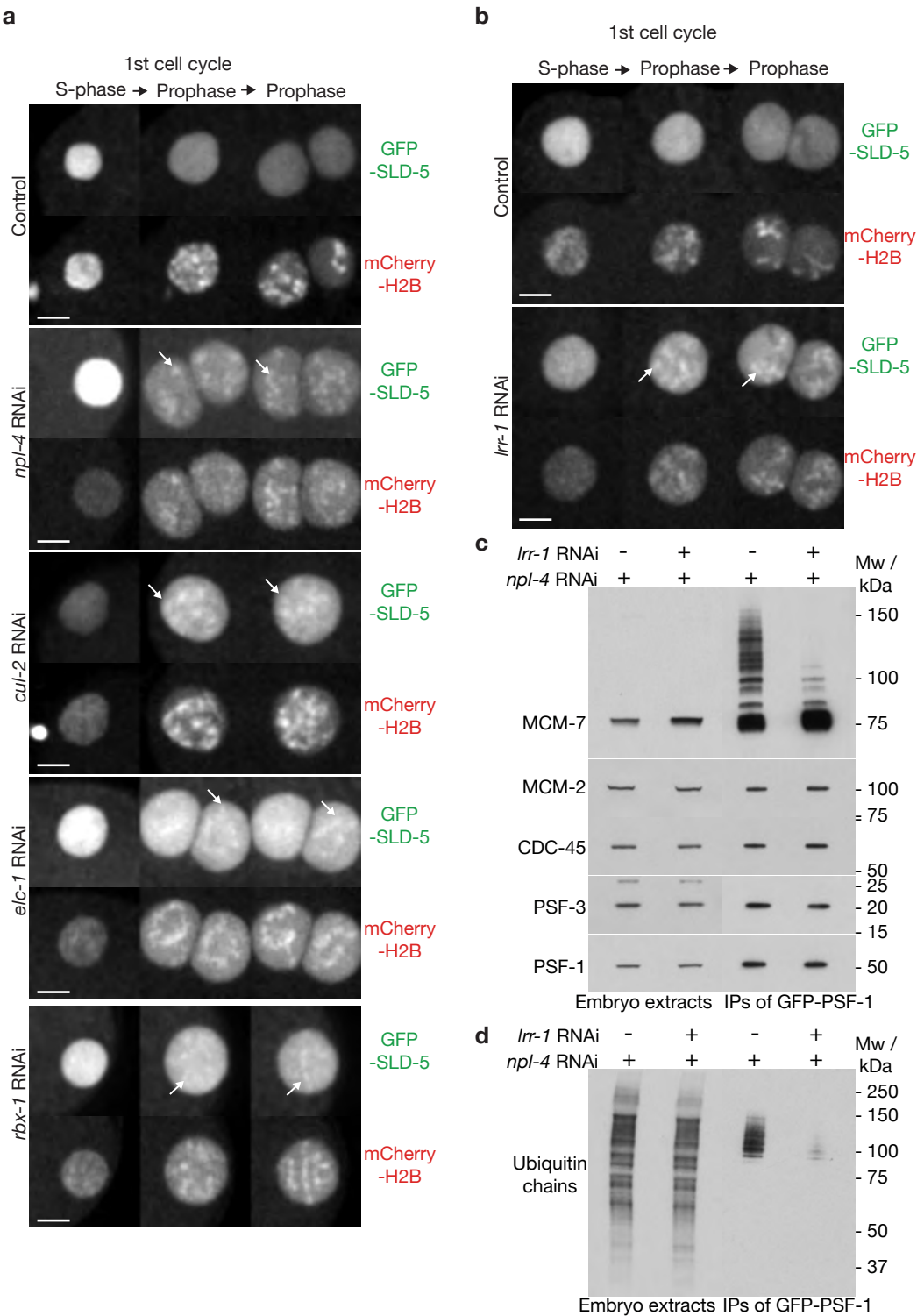
GFP-PSF-1 is released from chromatin before prophase in *ubxn-3* RNAi embryos. Images were acquired and analysed as for Supplementary Movie 1.

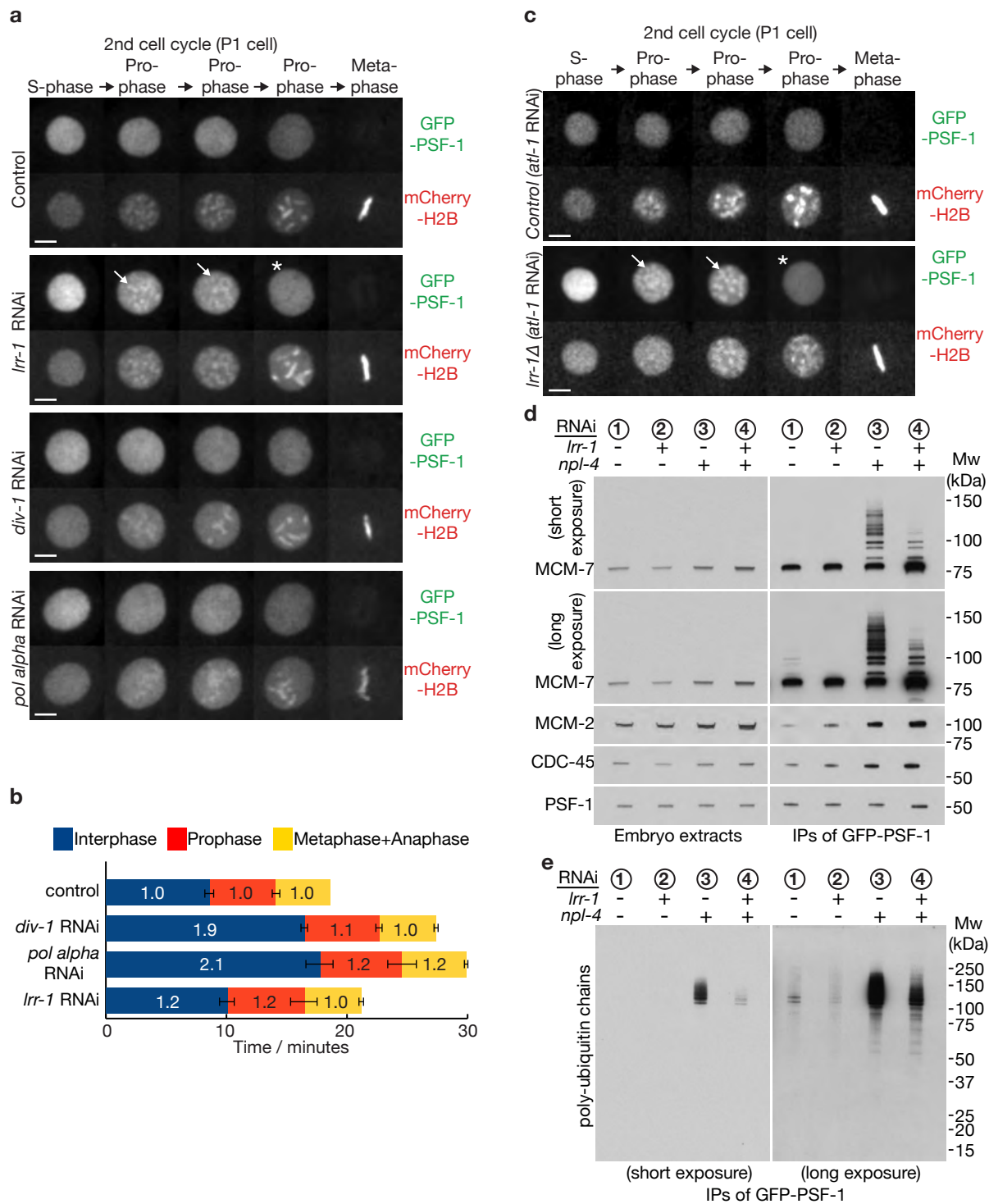
### **References**

1. Nguyen, H.C., Yang, H., Fribourgh, J.L., Wolfe, L.S. & Xiong, Y. Insights into Cullin-RING E3 ubiquitin ligase recruitment: structure of the VHL-EloBC-Cul2 complex. *Structure* **23**, 441-449 (2015).
2. Liu, J., Vasudevan, S. & Kipreos, E.T. CUL-2 and ZYG-11 promote meiotic anaphase II and the proper placement of the anterior-posterior axis in *C. elegans*. *Development* **131**, 3513-3525 (2004).
3. Sonnevile, R. & Gonczy, P. Zyg-11 and cul-2 regulate progression through meiosis II and polarity establishment in *C. elegans*. *Development* **131**, 3527-3543 (2004).

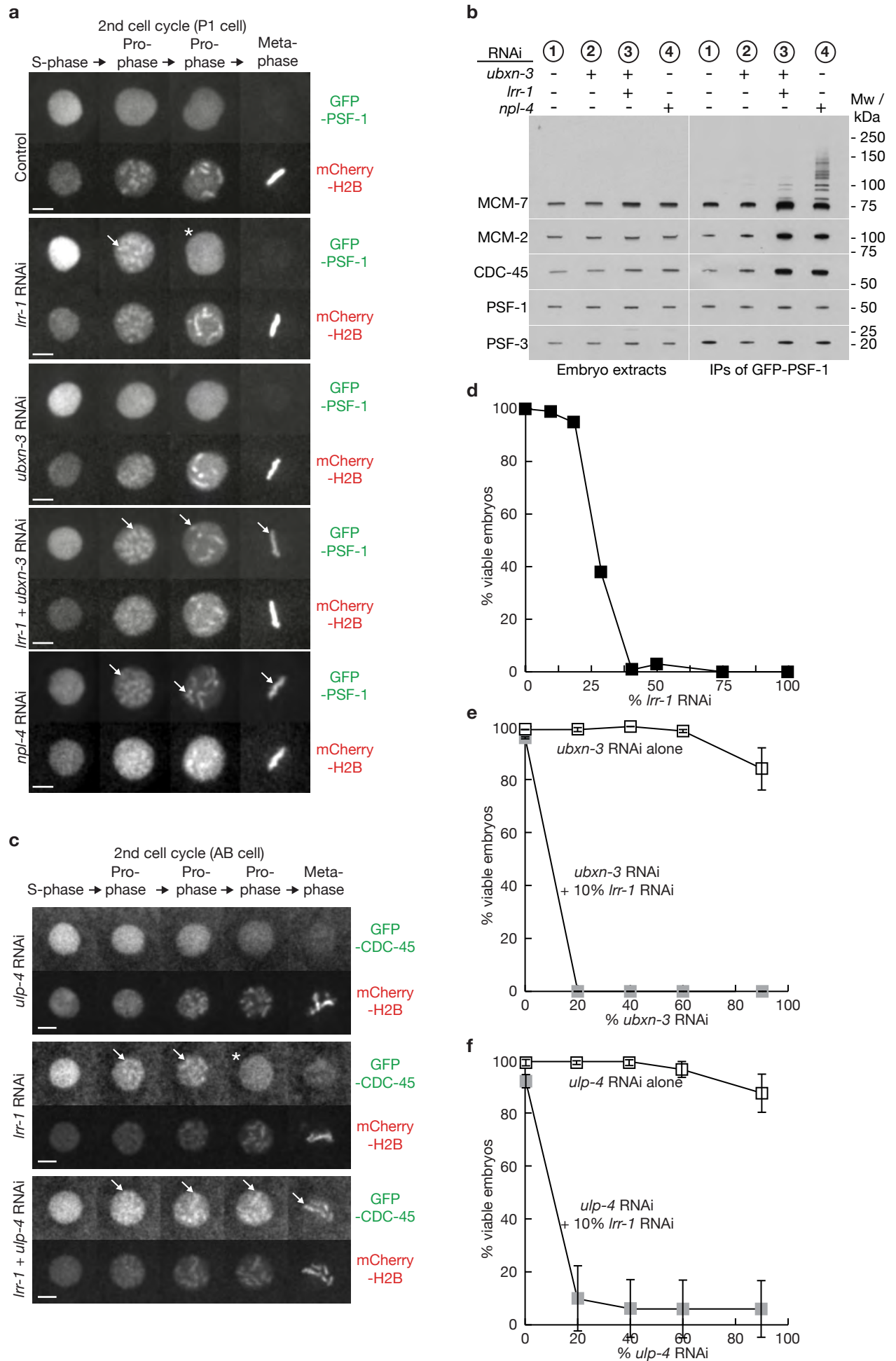


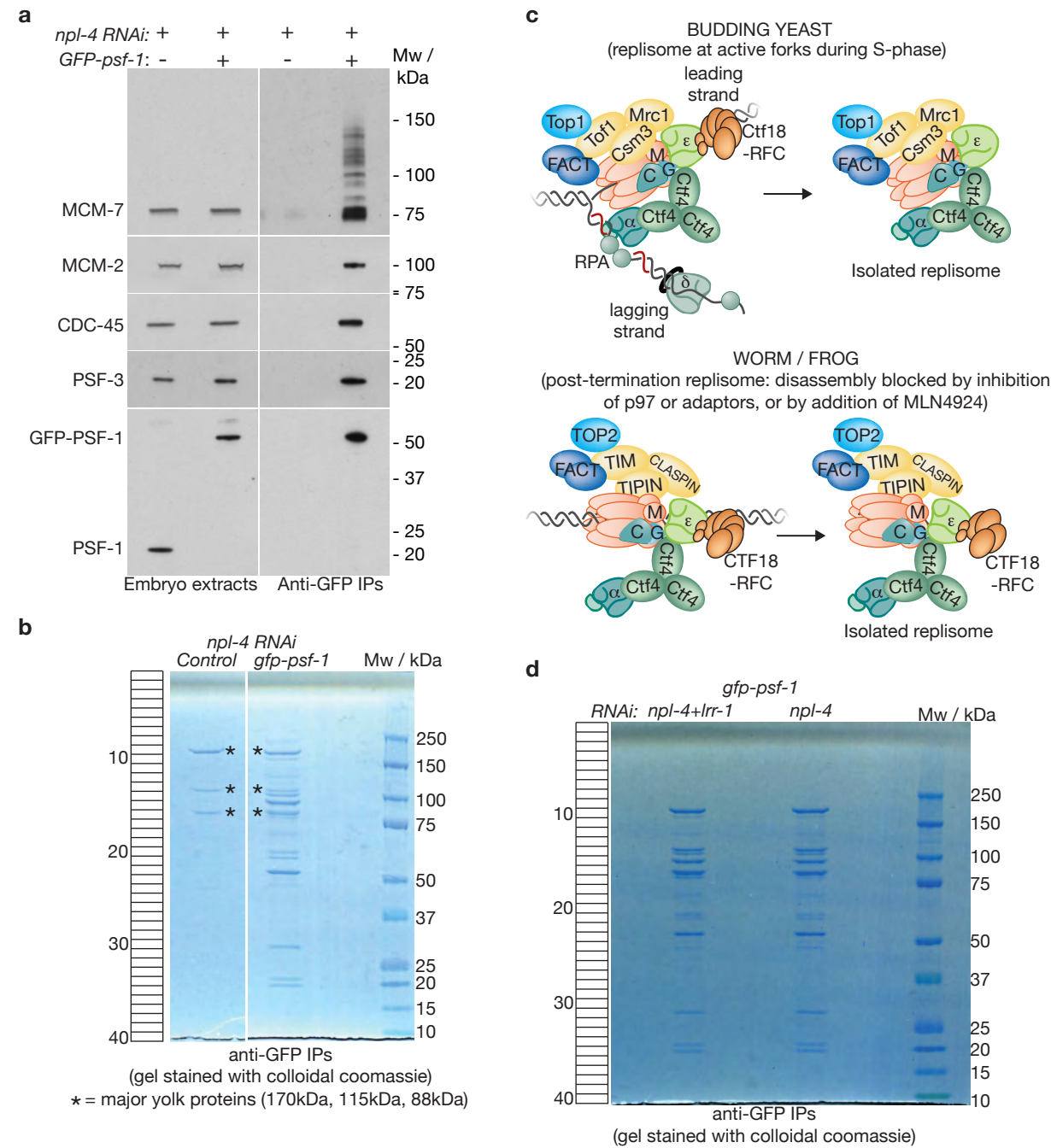
Sonneville et al Figure 2





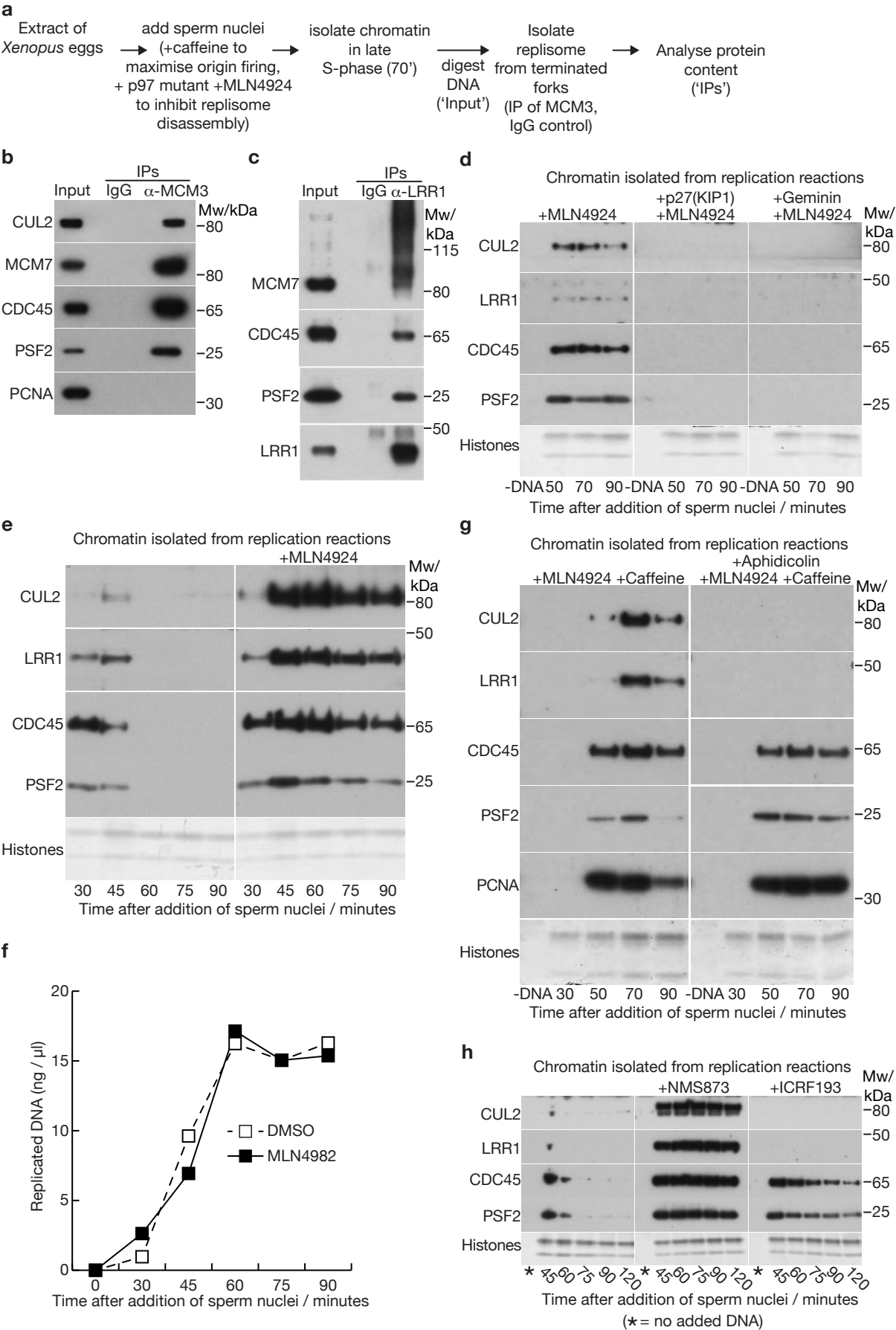
Sonneville et al Figure 4



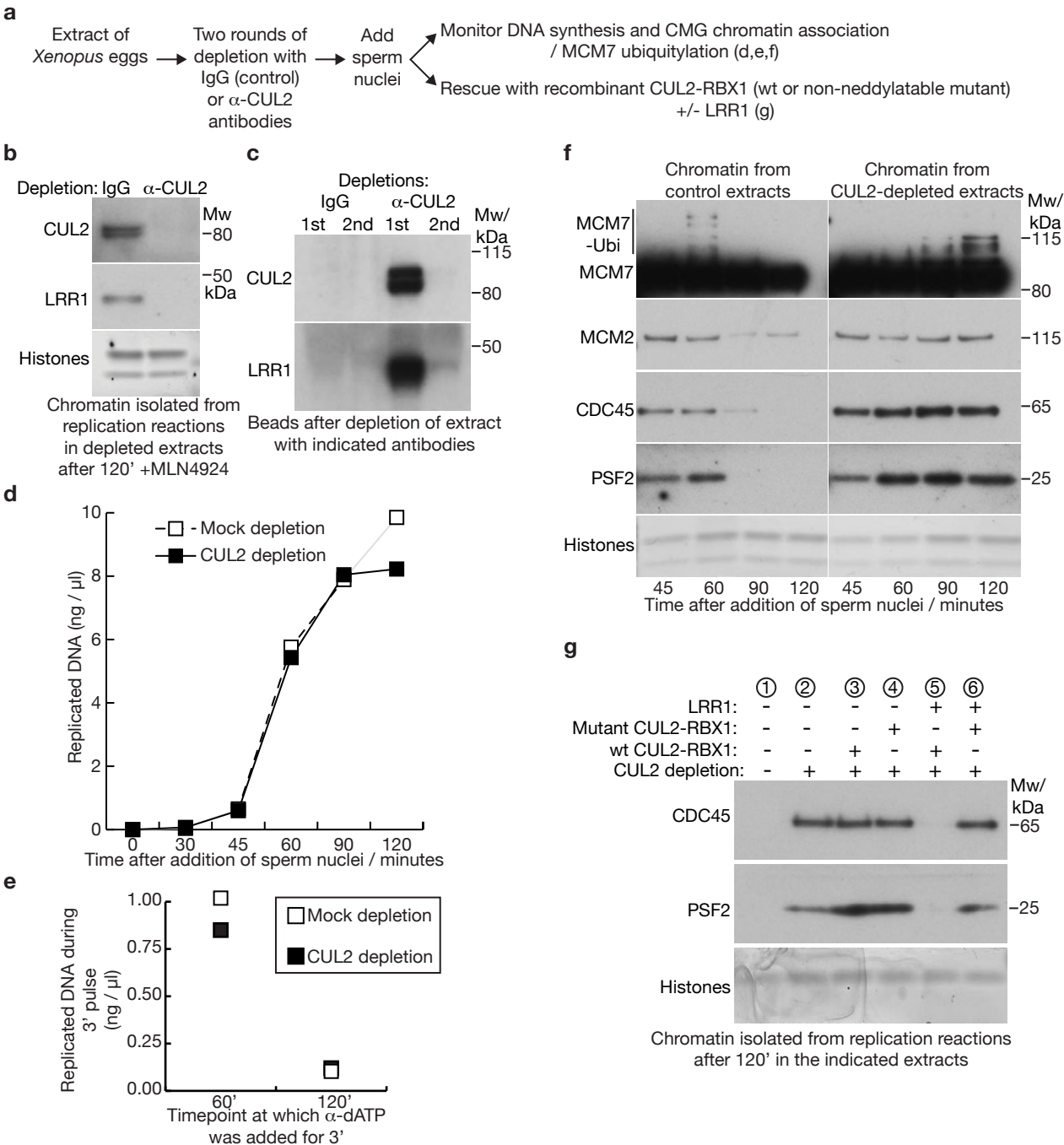


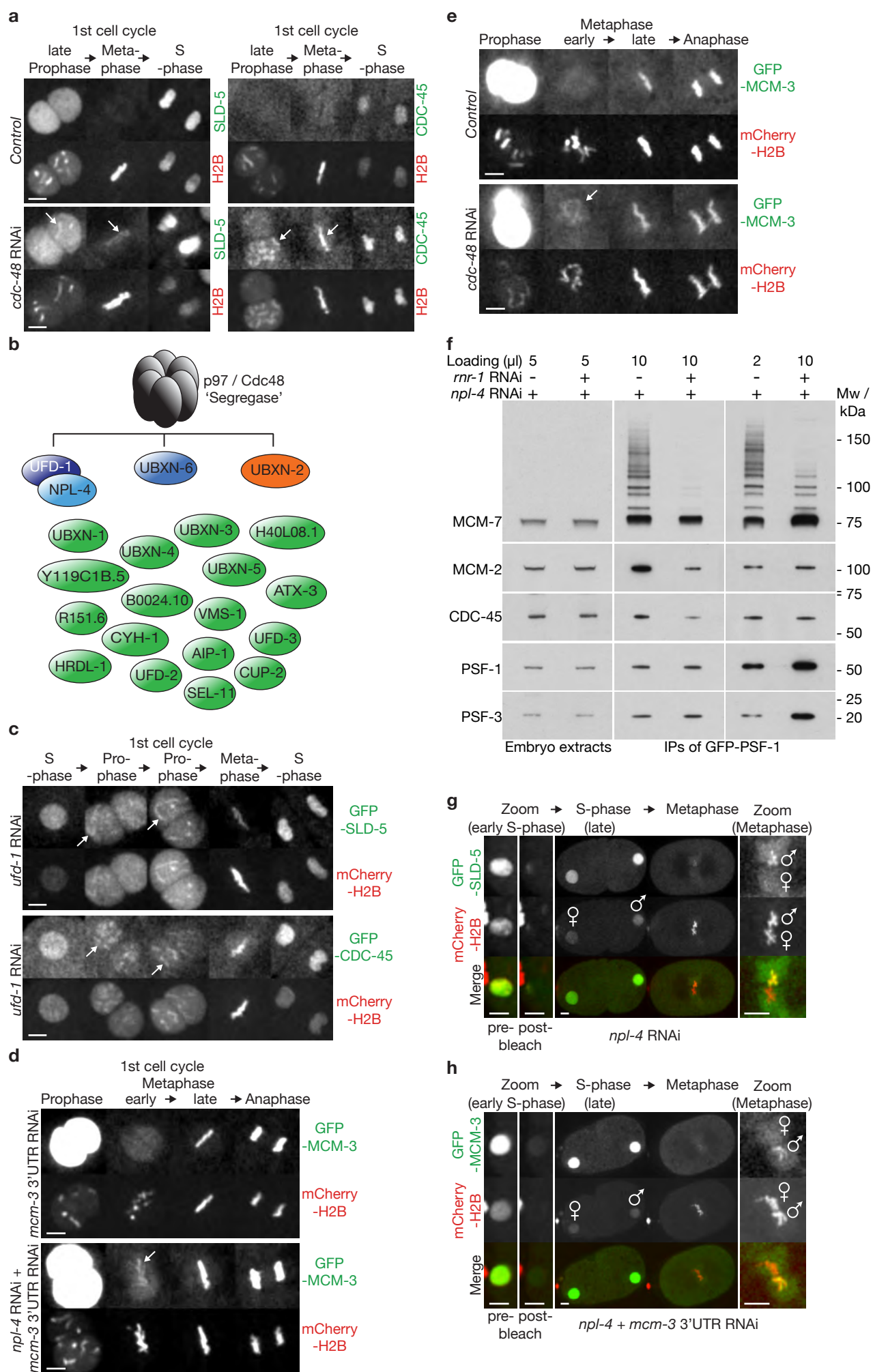


Sonneville et al Figure 6

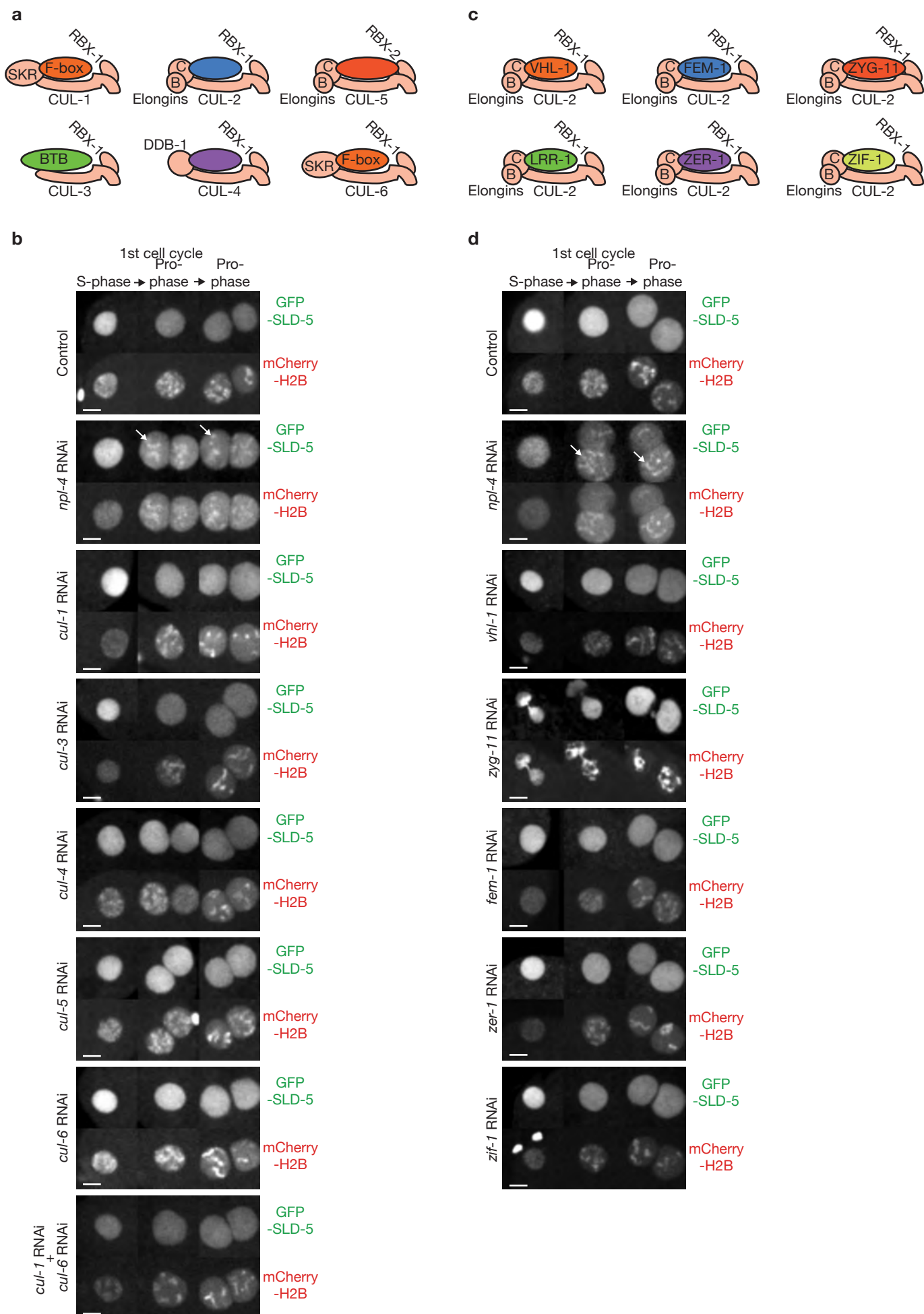


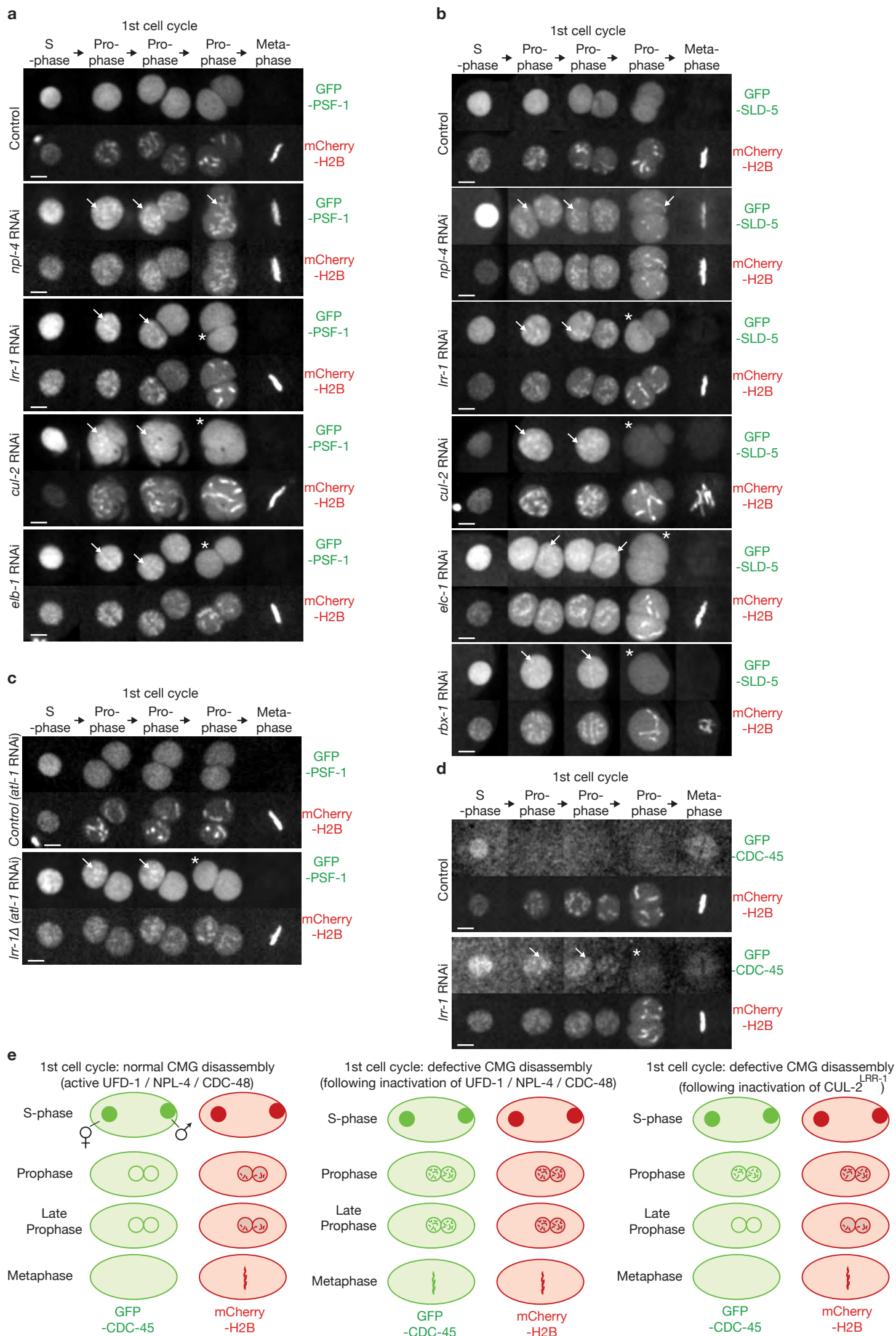






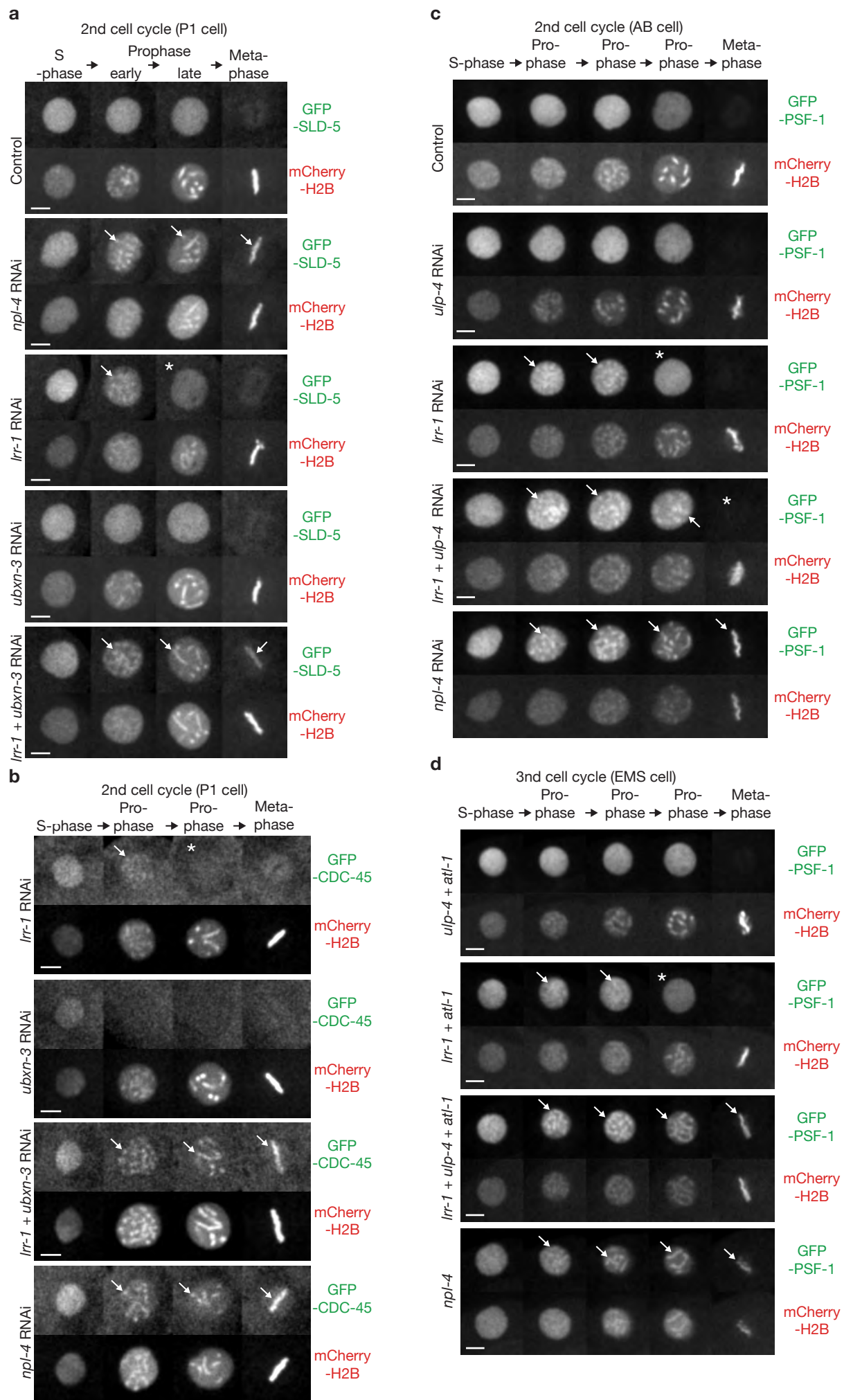
Sonneville et al Supplementary Figure 2

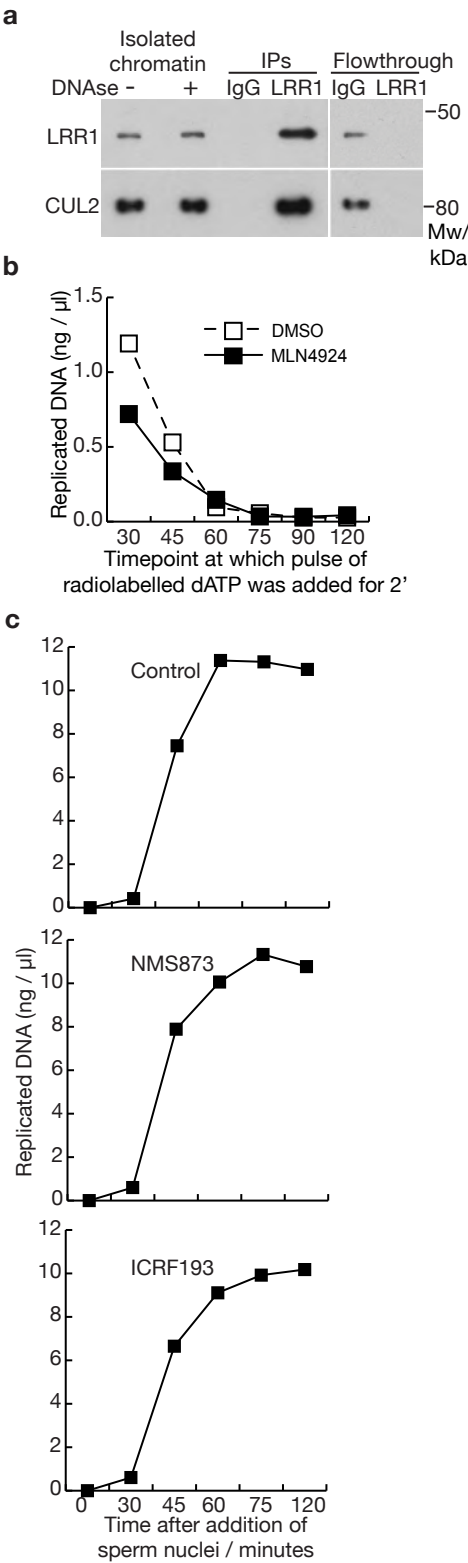






Sonneville et al Supplementary Figure 4





# Sonneville et al Supplementary Figure 6

Mm 1 MSLKPRVVDDETWNKLLTTIKAVVMLEYVERATWNRFSDIYALCVAYPEPLGERLYAETKIFLESHVRRHLYKRVLESEEQVLVMYHRY  
Hs 1 MSLKPRVVDDETWNKLLTTIKAVVMLEYVERATWNRFSDIYALCVAYPEPLGERLYTETKIFLENHVRHLHKRVLESEEQVLVMYHRY  
Xi 1 MSLKPRVVDDETWNKLLTTIKAVVMLDYVERATWNRFSDIYALCVAYPEPLGERLYTETKIFLENHVQQLHTRVLDSEAEQVLVMYFRY

Mm 91 WEEYSKGADYMDCLYRYLNTQYIKKNKLTEADIQYGYGGVDMNEPLMEIGELALDMWRKLMVEPLQNLILIRMLLREIKNDRGGEDPNQKV  
Hs 91 WEEYSKGADYMDCLYRYLNTQFIKKNKLTEADLQYGYGGVDMNEPLMEIGELALDMWRKLMVEPLQAAILIRMLLREIKNDRGGEDPNQKV  
Xi 91 WEEYSRGADYMDCLYRYLNTQYIKKNKLTEADLQYGYGGVDMNEPLMEIGELALDLWRKLMTEPLQDTLLILMLLREIKNDRGGEDPNQKV

Mm 181 IHGVINSFVHVEQYKKKFPKFKYQGIFVSPFLTETGEYYKQEASNLLQESNCSQYMEKVLGRLKDEEIRCRKYLHPSSYTKVIHECQORM  
Hs 181 IHGVINSFVHVEQYKKKFPKFKYQEIFESPFLTETGEYYKQEASNLLQESNCSQYMEKVLGRLKDEEIRCRKYLHPSSYTKVIHECQORM  
Xi 181 IHGVINSFVHVEQYKKKFPKFKYQEIFESPFLAETGEYYKQEASNLLQESNCSQYMEKILGRLKDEEIRCRKYLHPSSYNKVIHECQORM

Mm 271 VADHLQFLHSECHSIQQERKNDMANMYVLLRAVSSGLPHMIEELQKHHHDEGLRATSNLTQEHMPTLFVESVLEVHGKFPVLINTVLNG  
Hs 271 VADHLQFLHAECHNIIRQEKKNDMANMYVLLRAVSTGLPHMIQELQNHHDDEGLRATSNLTQENMPTLFVESVLEVHGKFPVLINTVLNG  
Xi 271 VADHLQFLHAECHNIIRQERRNDMANMYTLRAVSSGLPHMIQELQNHHDDEGLRAISNLSQENMPTQFVESVLEVHSGKFPVLVNCVLNG

Mm 361 DQHFMSALDKALTSVVNYREPKSVCAPPELLAKYCDNLLKKSAGKMTENEVEDKLTSPFITVFKYIDDKDVFQKFYARMLAKRLIHGLSMS  
Hs 361 DQHFMSALDKALTSVVNYREPKSVCAPPELLAKYCDNLLKKSAGKMTENEVEDRLTSPFITVFKYIDDKDVFQKFYARMLAKRLIHGLSMS  
Xi 361 DQHFMSALDKALTCVVNYREPKSVCAPPELLAKYCDNMLKKSAGKMTENEVEDKLTSPFITVFKYIDDKDVFQKFYARMLAKRLIHGLSMS

Mm 451 MDSEEMINKLKQACGYEFTSKLHRMYTDMSVSADLNNKFNNFIRNQDTVIDLGISFQIYVLQAGAWPLTQAPSSSTFAIPQELEKSVQMF  
Hs 451 MDSEEMINKLKQACGYEFTSKLHRMYTDMSVSADLNNKFNNFIKNQDTVIDLGISFQIYVLQAGAWPLTQAPSSSTFAIPQELEKSVQMF  
Xi 451 MDSEETMINKLKQACGYEFTSKLHRMYTDMSVSADLNNKFNNFISQDTVIDLGISFQIYVLQAGAWPLTQAPSSSTFAIPQELEKSVQMF

Mm 541 ELFYSQHFSGRKLTWLHLYLCTGEVKMNYLGKPYVAMVTYQMAVLLAFNNSETVSYKELQDSTQMNEKELTKTIKSLLDVKMINHDSKE  
Hs 541 ELFYSQHFSGRKLTWLHLYLCTGEVKMNYLGKPYVAMVTYQMAVLLAFNNSETVSYKELQDSTQMNEKELTKTIKSLLDVKMINHDSKE  
Xi 541 ELFYNQHFSGRKLTWLHLYLCTGEVKMNYLCKPYVAMVTYQMAVLLAFNNSEIITYKELQDSTQMNEKELTKTIKSLLDVKMINHDSKE

Mm 631 DIDAESSFSLNMSFSSKRTKFKITTSQKDTPOELEQTRSAVDEDRKMYLQAAIVRIMKARKVLRHNALIQEVISQSRARFNPSISMIKK  
Hs 631 DIDAESSFSLNMFSSKRTKFKITTSQKDTPOEMEQRSAVDEDRKMYLQAAIVRIMKARKVLRHNALIQEVISQSRARFNPSISMIKK  
Xi 631 DIEGESTFSLNMFSSKRTKFKITTPMQKDTPOEVEQTRSAVDEDRKMYLQAAIVRIMKARKVLRHNALIQEVISQSRARFNPSISMIKK

Mm 721 CIEVLIDKQYIERSQASADEYSYVA  
Hs 721 CIEVLIDKQYIERSQASADEYSYVA  
Xi 721 CIEVLIDKQYIERSQASADEYSYVA

<b>Protein</b>	<b>Properties</b>
AIR-2	Aurora protein kinase
PLK-1	Polo protein kinase
CYB-3	Cyclin B
CYA-1	Cyclin A
GSK-3	GSK3 protein kinase
MBK-2	MBK2 protein kinase
BRC-1	BRCA1 orthologue
BRD-1	BARD1 orthologue
D2085.4	HECT ligase (meiosis)
SMC-5	SMC5-6 complex
NSE-1	SMC5-6 complex
C32D5.10	RING (RNF146 orthologue)
C32D5.11	RING (Pex10 orthologue)
EEL-1	HECT ligase
Y47G6A.31	RING (homology with RNF4)
SPAT-3	RING (H2A ubiquitylation)
MIG-32	RING (H2A ubiquitylation)
RNF-113	RNF113 orthologue
VPS-11	VPS11 orthologue
TO1G5.7	RING (homology with RNF8)
ATL-1	ATR checkpoint protein kinase
ATM-1	ATM checkpoint protein kinase
SMC-4	Condensin
PIF-1	DNA helicase
DVC-1	Spartan protease
SMO-1	SUMO
UBC-9	SUMO E3 enzyme
ULP-4	Major mitotic SUMO protease



<b>Protein</b>	<b>Total spectral counts for control IP (npl-4 RNAi)</b>
MCM-2 (99 kDa)	62
MCM-3 (91 kDa)	167
MCM-4 (92 kDa)	87
MCM-5 (85 kDa)	137
MCM-6 (91 kDa)	70
MCM-7 (82 kDa)	150
CDC-45 (66 kDa)	12
PSF-1 (23 / 54 kDa)	3
PSF-2 (20 kDa)	15
PSF -3 (22 kDa)	2
SLD-5 (26 kDa)	0
CTF-4 (123 kDa)	12
SPT-16 (117 kDa)	14
SSRP-1A/B (79/78 kDa)	0 / 2
CTF-18 (97 kDa)	0
TIM-1 (157 kDa)	0
TIPIN (27 kDa)	0
TOPO-2 (172 kDa)	5
CLASPIN (85 kDa)	0
POLE1 (245 kDa)	37
POLE2 (59 kDa)	8
CUL-2 (98 kDa)	26
LRR-1 (51 kDa)	0

**Total spectral counts for PSF-1 IP (npl-4 RNAi)**

1244  
1110  
967  
1381  
1065  
1577  
563  
1624  
335  
399  
516  
  
94  
714  
124 / 229  
53  
624  
74  
37  
51  
211  
33  
  
156  
67

<b>Protein</b>	<b>Total spectral counts for PSF-1 IP (<i>npl-4</i> RNAi)</b>
MCM-2 (99 kDa)	585
MCM-3 (91 kDa)	655
MCM-4 (92 kDa)	493
MCM-5 (85 kDa)	682
MCM-6 (91 kDa)	483
MCM-7 (82 kDa)	1088
CDC-45 (66 kDa)	219
PSF-1 (23 / 54 kDa)	1033
PSF-2 (20 kDa)	274
PSF -3 (22 kDa)	319
SLD-5 (26 kDa)	338
CTF-4 (123 kDa)	64
SPT-16 (117 kDa)	246
SSRP-1A/B (79/78 kDa)	66 / 111
CTF-18 (97 kDa)	32
TIM-1 (157 kDa)	380
TIPIN (27 kDa)	51
TOPO-2 (172 kDa)	15
CLASPIN (85 kDa)	24
POLE1 (245 kDa)	51
POLE2 (59 kDa)	27
CUL-2 (98 kDa)	95
LRR-1 (51 kDa)	81

**Total spectral counts for PSF-1 IP (*lrr-1 npl-4* RNAi)**

800  
688  
552  
644  
630  
827  
211  
908  
217  
260  
203  
  
73  
343  
80 / 153  
12  
319  
16  
16  
20  
88  
29  
  
20  
5

<b>Protein</b>	<b>Total spectral counts for control IP</b>
MCM2 (100 kDa)	17
MCM3 (90 kDa)	17
MCM4 (97 kDa)	7
MCM5 (82 kDa)	30
MCM6 (93 kDa)	39
MCM7 (82 kDa)	24
CDC45 (66 kDa)	2
PSF1 (23 kDa)	0
PSF2 (21 kDa)	0
PSF 3 (24 kDa)	0
SLD5 (26 kDa)	0
CTF4 (125 kDa)	6
SPT16 (118 kDa)	3
SSRP (79 kDa)	0
TIMELESS (149 kDa)	0
TIPIN (40 kDa)	0
TOP2a (179 kDa)	6
CLASPIN (146 kDa)	0
POLA1 (165 kDa)	0
POLA2 (67 kDa)	0
POLE1 (261 kDa)	2
POLE2 (60 kDa)	0
CTF18 (113 kDa)	0
RFC3 (40 kDa)	4
RFC4 (40 kDa)	2
RFC2 (38 kDa)	0
p97 / CDC48 (89 kDa)	0
UFD1 (35 kDa)	0
NPL4 (69 kDa)	0
CUL2 (87 kDa)	0
LRR1 (47 kDa)	0
Elongin B (13 kDa)	0
Elongin C (12 kDa)	0

**Total spectral counts for MCM3 IP**

975

1111

947

927

888

905

277

62

33

55

44

554

453

229

171

54

484

72

109

7

543

103

172

36

31

27

361

4

19

101

46

5

7

<b>Protein</b>	<b>Total spectral counts for control IP</b>
CUL2 (87 kDa)	14
LRR1 (47 kDa)	8
Elongin B (13 kDa)	0
Elongin C (12 kDa)	0
MCM2 (100 kDa)	47
MCM3 (90 kDa)	47
MCM4 (97 kDa)	30
MCM5 (82 kDa)	46
MCM6 (93 kDa)	68
MCM7 (82 kDa)	50
CDC45 (66 kDa)	14
PSF1 (23 kDa)	2
PSF2 (21 kDa)	0
PSF 3 (24 kDa)	2
SLD5 (26 kDa)	2
CTF4 (125 kDa)	42
SPT16 (118 kDa)	29
SSRP (79 kDa)	6
TIMELESS (149 kDa)	0
TIPIN (40 kDa)	0
TOP2a (179 kDa)	20
CLASPIN (146 kDa)	2
POLA1 (165 kDa)	0
POLA2 (67 kDa)	0
POLE1 (261 kDa)	3
POLE2 (60 kDa)	4
CTF18 (113 kDa)	7
p97 / CDC48 (89 kDa)	0

**Total spectral counts for LRR1 IP**

748

197

20

26

275

252

190

243

251

216

128

25

17

21

25

350

136

40

62

26

283

107

17

2

145

31

29

16